Quantifying Quantum Chaos through Microcanonical Distributions of Entanglement

Joaquin F. Rodriguez-Nieva[1,*,†] Cheryne Jonay,[2,*] and Vedika Khemani[2]

[1]*Department of Physics and Astronomy, Texas A&M University, College Station, Texas 77843, USA*
[2]*Department of Physics, Stanford University, Stanford, California 94305, USA*

A characteristic feature of "quantum chaotic" systems is that their eigenspectra and eigenstates display universal statistical properties described by random matrix theory (RMT). However, eigenstates of local systems also encode structure beyond RMT. To capture this feature, we introduce a framework that allows us to compare the *ensemble* properties of eigenstates in local systems with those of pure random states. In particular, our framework defines a notion of distance between quantum state ensembles that utilizes the Kullback-Leibler divergence to compare the microcanonical distribution of entanglement entropy (EE) of eigenstates with a reference RMT distribution generated by pure random states (with appropriate constraints). This notion gives rise to a quantitative metric for quantum chaos that not only accounts for averages of the distributions but also higher moments. The differences in moments are compared on a highly resolved scale set by the standard deviation of the RMT distribution, which is exponentially small in system size. As a result, the metric can distinguish between chaotic and integrable behaviors and, in addition, quantify and compare the *degree* of chaos (in terms of proximity to RMT behavior) between two systems that are assumed to be chaotic. We implement our framework in local, minimally structured, Floquet random circuits, as well as a canonical family of many-body Hamiltonians, the mixed-field Ising model (MFIM). Importantly, for Hamiltonian systems, we find that the reference random distribution must be appropriately constrained to incorporate the effect of energy conservation in order to describe the ensemble properties of midspectrum eigenstates. The metric captures deviations from RMT across all models and parameters, including those that have been previously identified as strongly chaotic, and for which other diagnostics of chaos such as level spacing statistics look strongly thermal. In Floquet circuits, the dominant source of deviations is the second moment of the distribution, and this persists for all system sizes. For the MFIM, we find significant variation of the KL divergence in parameter space. Notably, we find a small region where deviations from RMT are minimized, suggesting that "maximally chaotic" Hamiltonians may exist in fine-tuned pockets of parameter space.

I. INTRODUCTION

The emergence of statistical mechanics from the dynamics of isolated quantum systems is a topic of fundamental interest [1–4]. While the foundations of this subject date back to the birth of quantum mechanics, the topic has seen a recent revival due to remarkable experimental advances in preparing isolated quantum systems that can be coherently evolved over unprecedented timescales [5–9]. Unlike in classical systems, notions of "ergodicity" and "chaos" in many-body quantum systems are much more ill defined. One prevailing approach to characterize quantum chaos is through the eigensystem properties of Hamiltonians (or time-evolution operators), specifically with respect to the emergence of universal behavior described by random matrix theory (RMT). This method applies both to correlations of eigenvalues, such as the level spacing statistics [10–12] or the spectral form factor [13–18], and to the properties of eigenstates. In particular, the central conjecture underpinning the celebrated eigenstate thermalization hypothesis (ETH) is that highly excited (infinite-temperature) eigenstates of chaotic quantum systems look like random pure states within subsystems [1–3,19–23]. This conjecture is reflected in the eigenstate expectation values of local observables [24,25], as well as the behavior of the eigenstate entanglement entropy (EE) [19,20,26–28].

In recent years, a series of works have used the von Neumann entanglement entropy to refine the correspondence

*These authors contributed equally to this work
†Contact author: jrodrieznieva@tamu.edu

between midspectrum eigenstates of local, physical Hamiltonians [29] (or Floquet systems) and random pure states (see Ref. [28] for a recent review). A widely prevailing expectation [28] is that—in the absence of additional conservation laws—infinite-temperature eigenstates of chaotic Hamiltonians (or eigenstates of chaotic Floquet systems) are nearly maximally entangled, with EE following the Page equation [30] derived for random pure states [Eq. (6)]. More recently, the Page result has been generalized to pure random states in various physically relevant *constrained* settings, in which the Hilbert space does *not* factor into a tensor product of the Hilbert spaces of subsystems [1,26,31–33]. Notable examples are systems with a local additive conserved charge, such as particle number, for which the Hilbert space is a direct sum of tensor products in different charge sectors. In this case, the typical EE for pure random states constrained to a given charge sector was recently derived analytically by Bianchi and Dona [31] and found in numerical studies to agree well with the eigenstate entropy of chaotic local Hamiltonians with particle-number conservation [28].

The fact that the eigenenergies and eigenstates of a wide range of nonrandom, sparse Hamiltonians numerically display universal RMT correlations (derived for random, dense matrices) is quite remarkable; understanding why this happens is a longstanding question in the study of quantum chaos. In particular, RMT ensembles, by design, have no spatial correlations while local Hamiltonians do. Furthermore, while a random many-body wave function in a system of size L has exponentially many [$O(\exp L)$] random parameters, a local Hamiltonian or Floquet unitary is specified with just polynomially many [$O(L)$] parameters.

Thus, various recent papers have focused on the question of how the eigenspectra of local systems encode structure beyond the leading-order RMT behavior, even in the absence of additional symmetries or constraints. For example, Refs. [34–38] have numerically and analytically studied systematic deviations between the EE of midspectrum Hamiltonian eigenstates and the Page entropy. Separately, Refs. [18,39–44] showed that matrix elements of local operators evaluated in the eigenbasis of Hamiltonian or Floquet systems are correlated up to certain energy scales (or inverse timescales related to, but possibly parametrically larger than, the so-called Thouless time); these works clarified that these correlations can be understood through the existence of a "light cone" in the growth of out-of-time ordered commutators in spatially local extended systems. In fact, eigenstates of local Hamiltonians "know" that they are *not* RMT: The correlations encoded in a single eigenstate suffice to reconstruct the entire Hamiltonian [19,45]. However, despite these various works, a systematic and unified understanding of eigenstate diagnostics of chaos, including universal deviations from RMT, is considerably less developed. This case is in contrast to eigenvalue diagnostics of chaos for which
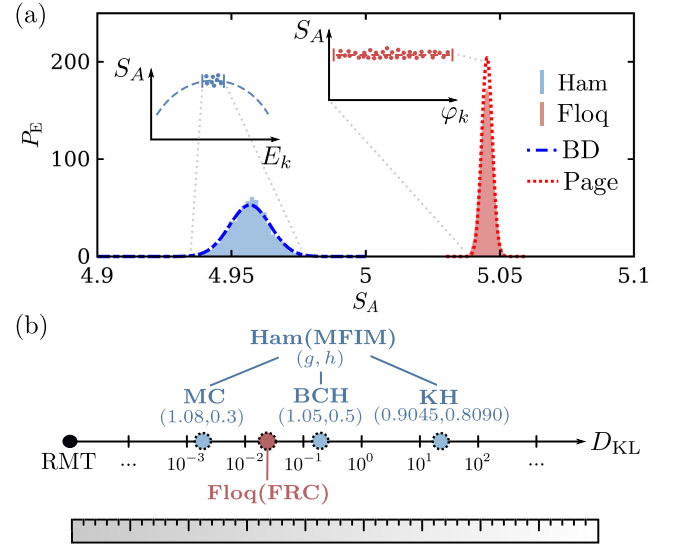

FIG. 1. (a) Histograms of EE of (left) midspectrum eigenstates of the mixed-field Ising model (MFIM) Hamiltonian [see Eq. (18)] and (right) eigenstates of a Floquet random circuit (FRC) with nearest-neighbor Haar random gates [see Eq. (10)]. The MFIM parameters are chosen to be strongly chaotic, with $g = 1.08$ and $h = 0.3$; FRCs are averaged over 50 circuit realizations. For comparison, we plot the reference RMT distributions, Page (dotted lines) and Bianchi-Dona (BD; dashed-dotted lines); see Secs. III A and IV A. We see that the former is the appropriate reference distribution for Floquet systems while the latter describes Hamiltonians with energy conservation. The reference distributions are plotted as Gaussian functions with analytically known means and standard deviations (see Appendix A). For all distributions, we consider a system of size $L = 16$ and a subsystem of size $L_A = 8$. (b) Distance between microcanonical distribution of eigenstate EE and RMT, as quantified through the KL divergence D_{KL}, Eq. (3). Shown are the values of D_{KL} plotted for a system of size $L = 16$ for the FRC and different MFIM parameters studied in the literature or discussed later in the main text: maximally chaotic (MC), Banulus-Cirac-Hastings (BCH) [48], and Kim-Huse (KH) [49]; see Fig. 4.

analytic results for the spectral form factor have been derived for various systems and have been shown to display RMT "ramp" behavior for times larger than the so-called Thouless time [13–18]. The Thouless time encodes the effects of locality and, in general, grows with system size; the Thouless time is minimized (and system-size independent) in certain "maximally chaotic" kicked-Ising Floquet models that are dual unitary [13,46,47].

Our perspective in this work is to compare the *ensemble* properties of eigenstates relative to RMT ensembles in order to quantify how chaotic a many-body Floquet or Hamiltonian systems is—in the sense of providing a continuous "ruler" measuring deviations from RMT (Fig. 1). The framework that we propose defines a measure of "distance" to the appropriate RMT ensemble by computing the Kullback-Leibler (KL) divergence, $D_{KL}(P_E, P_R)$, between the microcanonical distribution of eigenstate EE,

$P_{\mathrm{E}}(S_A)$, and an appropriate reference RMT distribution, $P_{\mathrm{R}}(S_A)$. Here, S_A refers to the EE of a subsystem A of a pure state, which is chosen to be either an eigenstate or a random state. In other words, we ask how well the microcanonical ensemble of eigenstates reproduces the distribution of EE generated by an (appropriately constrained) ensemble of random pure states. For Hamiltonian systems, the micro-canonical ensemble is obtained from a narrow window of eigenstates centered at infinite temperature, while we use the entire eigenspectrum for Floquet systems.

Importantly, the framework that we introduce compares ensemble properties *beyond* the first moment by also incorporating higher moments of the distributions, which depend on the fluctuations of EE across eigenstates. In fact, we show that these fluctuations play a key role and capture deviations from RMT that may not be visible in the first moment in certain systems. In addition, because D_{KL} employs the same baseline distribution for all Hamiltonians, we can quantify and compare the degree of quantum chaos of two different systems assumed to be chaotic using the same ruler D_{KL}. In particular, we say that system A is more chaotic (or has a larger "degree of chaos") than system B if all the moments of the eigenstate distributions of system A are closer to the RMT expectation values than those of system B; see Fig. 1(b). [50] As we will see, this case will allow us to identify special Hamiltonians in a broad landscape of local physical systems that behave almost RMT-like.

A. Summary of results

We study two models in this work: local FRCs and a family of MFIM Hamiltonians parametrized by the strength of the transverse and longitudinal fields. Our main results are summarized as follows.

First, in minimally structured FRCs (which only retain locality and have no other structure or conservation laws), we find that the dominant contribution to D_{KL} comes from the microcanonical fluctuations of EE. In particular, we find that σ_{E}, the standard deviation of the micro-canonical distribution, is systematically larger than σ_{R}, the standard deviation of the Page distribution, which is the reference RMT distribution. In contrast, the means μ_{E} and μ_{R} are much better converged. We note that D_{KL} furnishes a very finely resolved comparison between the microcanon-ical and RMT distributions by normalizing the differences between the distributions by σ_{R}, so the contributions of the first two moments of the microcanonical distribution to D_{KL} are functions of the ratios $|\mu_{\mathrm{E}} - \mu_{\mathrm{R}}|/\sigma_{\mathrm{R}}$ and $\sigma_{\mathrm{E}}/\sigma_{\mathrm{R}}$; see Eq. (4). For the reference RMT distribution, the standard deviation is exponentially small in system size: $\sigma_{\mathrm{R}} \sim \sqrt{2^{-L}}$. Thus, unlike prior works, D_{KL} not only measures whether $|\mu_{\mathrm{E}} - \mu_{\mathrm{R}}|$ decreases with system size, or whether σ_{E} displays exponentially small scaling similar to RMT, but rather, it probes these differences on the exponentially small scale set by σ_{R}. For FRCs, we find that

the difference in mean between the microcanonical and RMT distributions is small even on the scale of σ_{R}, while the ratio $\sigma_{\mathrm{E}}/\sigma_{\mathrm{R}}$ shows a sizable and positive $O(1)$ departure from 1 that appears stable with system size (Fig. 2). In other words, for FRCs, we find that $\sigma_{\mathrm{E}} \sim \sqrt{2^{-L}}$ but with a systematically larger prefactor than the reference Page distribution. We attribute this relative increase in σ_{E} to locality since FRCs do not have any structure or sym-metries beyond locality and time periodicity.

Second, even for Hamiltonian systems, we find that the difference between the microcanonical and RMT prediction is exponentially small in system size (and comparable to σ_{R} in large regions of parameter space, away from integra-bility), provided we suitably constrain the RMT ensemble. This case may seem at odds with various works that recently noted that the EE of midspectrum Hamiltonian eigenstates shows a small but systematic $O(1)$ negative departure from the Page value [34–38]. Remarkably, we show instead that the departure is captured if we instead compare μ_{E} to the mean of the BD distribution [31] obtained for systems with a local $U(1)$ charge. In other words, a "better" RMT ensemble for describing midspec-trum eigenstates of local Hamiltonians is the BD distribu-tion (as opposed to the Page distribution): Energy conservation plays the role of an additive local charge—even at infinite temperature and in the absence of addi-tional symmetries such as particle number conservation—and the BD distribution incorporates this important feature (see Fig. 1). This result is of independent interest, and it updates numerous prior studies in which midspectrum eigenstates of local Hamiltonians (without additional symmetries) have been compared to the Page distribution [28]. We note that the deviation between the average microcanonical EE for Hamiltonian systems and the Page entropy was also previously argued by Huang in Refs. [35,36], agreeing with the results obtained by using the BD ensemble. In Fig. 1, we plot the microcanonical EE distribution for a nonintegrable Hamiltonian and Floquet random circuit, and show that they are well described (to leading order) by the BD and Page distri-butions, respectively. In particular, Fig. 1 shows that the means of the two reference RMT distributions differ by about 0.1, which entirely captures the $O(1)$ deviation from Page that was previously observed for the EE of Hamiltonian eigenstates [34–36].

Third, for Hamiltonian systems, we find that D_{KL} shows significant variation in parameter space for the models and system sizes we study—even in parameter regimes where other metrics of chaos such as level statistics have saturated to the RMT predictions (Fig. 4). Remarkably, there are small islands in parameter space that minimize D_{KL}, and these are quite far in parameter space from "standard" reference values that are widely used in studies of chaos in the MFIM, such as the Kim-Huse parameters of Ref. [49]. At the strongly chaotic points, the deviations in both

$|\mu_E - \mu_R|/\sigma_R$ and σ_E/σ_R are comparable, while these differences steeply increase away from the maximally chaotic regions, resulting in a large D_{KL}. As such, our FRC and Hamiltonian results show that D_{KL} can resolve differences in microcanonical and RMT distributions, even if the moments of the former are "exponentially close" to the latter. This variation in parameter space suggests that there might be "maximally chaotic" Hamiltonians in judiciously tuned regions of parameter space, similar to maximally chaotic dual-unitary Floquet circuits [13,46,47] or minimally chaotic integrable models, with the degree of chaos attainable being constrained by features such as locality or the type of allowed interactions.

More generally, the approach to compare microcanonical and RMT distributions, including higher moments, is reminiscent of (but different in detail from) studies of unitary and state design in quantum information theory [51–56]. For example, studies of k-design formation compare the lowest k moments of candidate probability distributions over a unitary group against the uniform Haar distribution; this approach is particularly informative in understanding distributions for which the lower moments agree with the Haar distribution while higher moments show deviations. Likewise, a notable feature of our work is that the microcanonical standard deviation of EE is informative in characterizing chaos even in models where the mean agrees with RMT predictions.

There are also practical advantages of quantifying chaos through the microcanonical statistics of entanglement entropy. A single Hamiltonian produces its own microcanonical ensemble of eigenstates, which is then used to characterize chaos. This case contrasts with other metrics like the spectral form factor, which requires sampling over Hamiltonian ensembles [57]. It also makes the approach quantitative as it allows one to compare the distance to RMT for two different systems using the same well-characterized benchmark. Furthermore, only a relatively small number of eigenstates are required to characterize the distribution of EE up to the second moment, therefore making the method inexpensive and relatively easy to implement for relatively large system sizes through various shift-invert or polynomial filtering techniques for targeting eigenstates in small energy or quasienergy windows [58,59]. Finally, our metric of chaos is intrinsic to eigenstates and is therefore operator independent, unlike methods that rely on susceptibility metrics, which require specifying a perturbing operator [60].

The outline of the rest of this paper is as follows. In Sec. II, we introduce our metric for quantum chaos and describe its behavior in simple limits. In Sec. III, we begin the discussion by introducing the relevant RMT distribution that will be used to quantify chaos in Floquet random circuits, namely, the Page distribution. We then present numerical results for the distribution of EE of eigenstates in

minimally structured Floquet random circuits and discuss contributions of the first two moments to the distance measure. In Sec. IV, we begin by introducing the relevant RMT distribution that will be used to quantify chaos in Hamiltonian systems, namely, the BD distribution. We then present numerical results for the MFIM, a paradigmatic Hamiltonian system that exhibits both integrable and chaotic regimes. We discuss the behavior of the eigenstate EE distribution in the proximity of maximally chaotic parameters, as well as the differences with respect to other metrics of chaos employing spectral statistics. Finally, in Sec. V, we summarize the main results of our work and discuss directions for future work.

II. QUANTIFYING QUANTUM CHAOS

Our goal is to quantify the proximity of a given Hamiltonian or Floquet unitary to RMT behavior by comparing the microcanonical distribution of eigenstate EE, $P_E(S_A)$, with a reference distribution for the EE of (appropriately constrained) pure random states, $P_R(S_A)$. We consider systems of size L and Hilbert space dimension d partitioned into two subsystems A and B with sizes $L_A \leq L_B$, respectively. We find it convenient to introduce the ratio $f = L_A/L \leq 1/2$. All the numerical data in this work will be for one-dimensional spin-$1/2$ systems, but the methods readily generalize to higher dimensions and systems of qudits.

To obtain the microcanonical distribution, we choose eigenstates $|k\rangle$ of the Floquet or Hamiltonian systems with energy/quasienergy E_k/φ_k, respectively. The reduced density matrix obtained from eigenstate $|k\rangle$ is

$$\rho_{A,k} = \text{Tr}_B[\rho_k], \qquad \rho_k = |k\rangle\langle k|, \tag{1}$$

with associated von Neumann entanglement entropy

$$S_{A,k} = -\text{Tr}[\rho_{A,k} \log \rho_{A,k}]. \tag{2}$$

For Hamiltonian systems, we construct the microcanonical distribution $P_E(S_A)$ by computing the EE of eigenstates in a small window centered around the middle of the spectrum, i.e., at an energy density corresponding to infinite temperature (details are discussed in Sec. IV). For Floquet unitaries, there is no conserved energy or notion of temperature (or, colloquially, all states are at infinite temperature); therefore, the full eigenbasis corresponding to states at all quasienergies is used to construct $P_E(S_A)$.

Our goal is to define a distance between the microcanonical distribution $P_E(S_A)$ and a reference random distribution $P_R(S_A)$. A natural choice for the distance between distributions is the KL divergence,

$$D_{\mathrm{KL}}(P_{\mathrm{E}}, P_{\mathrm{R}}) = \int dS_A P_{\mathrm{E}}(S_A) \log \frac{P_{\mathrm{E}}(S_A)}{P_{\mathrm{R}}(S_A)} \geq 0. \quad (3)$$

The KL divergence is the expectation of the logarithmic difference between probability distributions, and it is a measure of the information loss when the reference distribution $P_{\mathrm{R}}(S_A)$ is used to approximate the empirical eigenstate distribution $P_{\mathrm{E}}(S_A)$. The KL divergence is a type of distance since it is always non-negative and takes value 0 when the reference and empirical distribution are equal. However, it is not a metric distance because it is asymmetric in the two distributions and does not satisfy the triangle inequality.

Let us evaluate Eq. (3) in a simple yet important limit. Given the first two moments $\mu_{\mathrm{E/R}}$ and $\sigma_{\mathrm{E/R}}$ of the empirical (eigenstate) and reference (or random state) distributions, we make a Gaussian approximation for both $P_{\mathrm{E}}(S_A) \approx (1/\sqrt{2\pi\sigma_E^2}) \exp\{-[(S_A - \mu_{\mathrm{E}})^2/2\sigma_E^2]\}$ and $P_{\mathrm{R}}(S_A) \approx (1/\sqrt{2\pi\sigma_R^2}) \exp\{-[(S_A - \mu_{\mathrm{R}})^2/2\sigma_R^2]\}$. Within this approximation, D_{KL} quantifies the difference between means (relative to σ_{R}) and the ratio $\sigma_{\mathrm{E}}/\sigma_{\mathrm{R}}$ through the nonlinear relations

$$D_{\mathrm{KL}} = D_{\mathrm{KL}}^{(1)} + D_{\mathrm{KL}}^{(2)},$$
$$D_{\mathrm{KL}}^{(1)} = \frac{(\mu_{\mathrm{E}} - \mu_{\mathrm{R}})^2}{2\sigma_{\mathrm{R}}^2},$$
$$D_{\mathrm{KL}}^{(2)} = \frac{1}{2}\left[\left(\frac{\sigma_{\mathrm{E}}}{\sigma_{\mathrm{R}}}\right)^2 - 1\right] - \log\frac{\sigma_{\mathrm{E}}}{\sigma_{\mathrm{R}}}. \quad (4)$$

In what follows, we make this Gaussian approximation and only focus on the first two moments for the reference and empirical distributions while computing D_{KL}. While this is not strictly accurate (the strict upper bound on the value of entropy produces a skewness, for instance, which has been computed for random states with and without charge conservation symmetry [31]), it is still a good approximation because the higher moments scale with increasing powers of $1/d$, where d is the Hilbert space dimension [31].

The different $P_{\mathrm{R}}(S_A)$ studied in this work, i.e., the Page and Bianchi-Dona distributions, will be discussed in the following sections. Both distributions have $\sigma_{\mathrm{R}} \sim \sqrt{2^{-L}}$; thus, as mentioned earlier, D_{KL} provides a highly resolved comparison between the microcanonical and reference RMT distributions by comparing the differences between their moments on the exponentially small scale set by σ_R, as seen by the expressions for $D_{\mathrm{KL}}^{(1,2)}$ in Eq. (4).

As a final remark, we note that the choice of entanglement observable to be used in Eq. (3) is not important for the purposes of the present work. In particular, we focus on the von Neumann entanglement entropy as it is a well-established and well-understood quantity. However, other entanglement observables could have been used, such as the Renyi entropy $S_n = (1/1 - n) \log(\mathrm{Tr}[\rho_A^n])$, or even the entire entanglement spectrum. In fact, certain entanglement observables, especially the second Renyi entropy ($n = 2$), are easier to measure in ongoing experiments [6]. In the Appendix F, we show that all the conclusions obtained using the von Neumann EE S_A are also true when calculations are performed using the second Renyi entropy S_2.

III. FLOQUET SYSTEMS

We start by analyzing a minimally structured model of chaotic thermalizing dynamics, namely, Floquet random circuits that only feature locality and no other conservation laws. In the absence of energy or $U(1)$ conservation, we employ the Page distribution as the reference RMT distribution. We include a discussion of $\mu_{\mathrm{R}}, \sigma_{\mathrm{R}}$ for the Page distribution for completeness and to set notation, before presenting our numerical results.

A. Reference distribution I: Page distribution

We begin by recapitulating the Page distribution for the bipartite entanglement entropy of pure random states chosen uniformly with respect to the Haar measure, unconstrained by symmetry. Our nomenclature takes some historical liberties: In fact, Page only conjectured (and partially proved) the expression for the first moment of this distribution [30]; explicit derivations for the first and higher moments were later furnished in Refs. [31,61,62].

As mentioned above, we focus on the first two moments of the Page distribution in this work. The exact analytical expressions for these moments (for finite system sizes) are reproduced in Appendix A and used in our numerical comparisons below. We briefly discuss these expressions in the limits $L_A, L_B \gg 1$ and when $0 < f \leq 0.5$ is a finite fraction as $L \to \infty$. The first moment in this limit is approximated as

$$\langle S_A \rangle_{\mathrm{P}} \equiv \mu_{\mathrm{P}}(f) \approx \log(d_A) - \frac{d_A}{2d_B}, \quad (5)$$

where d_A and d_B refer to the Hilbert space dimensions of subsystems A and B, respectively. We henceforth use the subscript "P" for Page in order to denote moments computed with respect to the Haar measure. For a system of qubits, this reduces to

$$\mu_{\mathrm{P}}(f) \approx fL\log(2) - 2^{-L(1-2f)-1}. \quad (6)$$

The first term is the volume law term, which describes an entanglement entropy scaling with the size of subsystem A, $L_A = fL$, while the second term is the Page correction, which is exponentially small when $f < 1/2$. For $f = 1/2$, it gives rise to a "half-bit" shift:

$$\mu_{\mathrm{P}}\left(f = \frac{1}{2}\right) \approx \frac{L}{2}\log(2) - \frac{1}{2}. \quad (7)$$

More recently, the second moment of the distribution was calculated using various techniques [31,61,62] and, in the limit $L_A, L_B \gg 1$, is approximated as [28]

$$\sigma_{\mathrm{P}}^2(f) \approx \left(\frac{1}{2} - \frac{1}{4}\delta_{f,\frac{1}{2}}\right)\frac{1}{d_B^2} = \left(\frac{1}{2} - \frac{1}{4}\delta_{f,\frac{1}{2}}\right)2^{-2L(1-f)}. \quad (8)$$

The second moment of the distribution σ_{P} is exponentially small in L and scales as $\sqrt{1/d}$ at $f = 1/2$:

$$\sigma_{\mathrm{P}}\left(f = \frac{1}{2}\right) \approx \frac{1}{2}\sqrt{2^{-L}}. \quad (9)$$

Because $\sigma_{\mathrm{P}}/\mu_{\mathrm{P}} \ll 1$, a *typical* random state will have EE given by Eq. (6).

B. Numerical results

We consider a Floquet random unitary circuit comprised of two layers of Haar random two-site unitary gates acting on odd and even bonds, $U_F = U_{\mathrm{odd}}U_{\mathrm{even}}$, in a spin-1/2 chain of even length L with periodic boundary conditions:

$$U_{\mathrm{even}} = U_{0,1} \otimes U_{2,3} \otimes U_{4,5} \cdots \otimes U_{L-2,L-1},$$
$$U_{\mathrm{odd}} = U_{1,2} \otimes U_{3,4} \otimes U_{5,6} \cdots \otimes U_{L-1,0}. \quad (10)$$

Each of the unitary matrices $U_{i,i+1}$ is chosen randomly and uniformly from the Haar measure on $U(4)$. The time-evolution operator for integer times t is $U(t) = U_F^t$. We emphasize that the system has locality and time periodicity but no additional symmetries.

The microcanonical EE distribution $P_{\mathrm{E}}(S_A)$ is computed as a function of L for $L_A = L/2$ and compared with the Page distribution of EE for pure random states. The mean and standard deviation of the EE distribution are denoted μ_U and σ_U, respectively, where we use the subscript U to denote eigenstates of unitary circuits, which is more descriptive than the μ_{E} and σ_{E} symbols introduced in Sec. II (which referred collectively to moments of eigenstate distributions of either Hamiltonian or Floquet systems). For each system size, we average the microcanonical EE distribution over 50 circuit realizations and compute the microcanonical distribution from the entire Floquet spectrum for a given realization. For $L \leq 14$, we use exact diagonalization to compute all eigenvectors and quasienergies for U_F. For $L = 16$, we use the polynomial filtering diagonalization method introduced in Ref. [59] to obtain a total of 2000 eigenstates per circuit. These eigenstates are obtained in groups of 50 states centered around 40 evenly spaced quasienergies distributed across the full quasienergy spectrum. In Appendix B, we show that our results are not sensitive to whether the microcanonical distribution is obtained using the full spectrum vs narrower windows of states clustered around particular quasienergies.

In Fig. 1(a), we show that the distribution $P_{\mathrm{E}}(S_A)$ for $L = 16$ and $L_A = 8$ shows good agreement with the Page
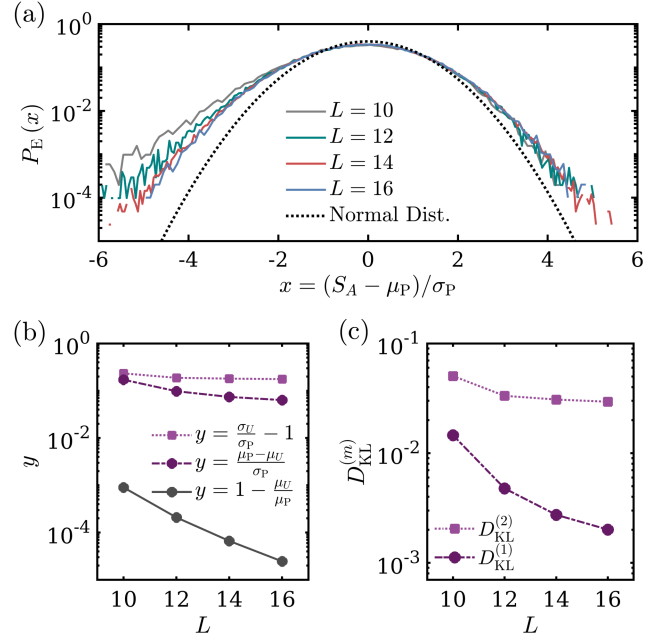

FIG. 2. (a) Histogram of eigenstate EE for a FRC as a function of system size showing a broader distribution than that predicted by RMT; see also Fig. 1. The standard normal distribution is shown with dotted lines. (b) System-size scaling of the first two moments of the EE distribution relative to RMT behavior. Shown is the convergence of differences in EE means (plotted both relative to μ_{P} and to σ_{P}) while finite deviations of standard deviations persists for all system sizes. (c) Contributions to D_{KL} by the first two moments of the EE distribution of FRC eigenstates.

distribution, so the entanglement properties of eigenstates of FRCs are well described by the entanglement properties of Haar random states, as expected from numerous prior works. We now provide a more finely resolved comparison of the microcanonical and Page distributions for different system sizes; in particular, we compare both the first and second moments of these distributions and probe differences on the exponentially small scale set by σ_{P}. For each eigenstate, we shift the EE of the eigenstate by μ_{P} and normalize by σ_{P} [the expressions for μ_{P} and σ_{P} depend on L and are provided in Eqs. (A3) and (A4)]. With these transformations, the Page distribution (within the Gaussian approximation) reduces to a standard normal distribution for all L. The shifted and rescaled distributions for $x = (S_A - \mu_{\mathrm{P}})/\sigma_{\mathrm{P}}$ are plotted in Fig. 2(a), with the standard normal distribution shown for comparison. We see from this figure that, while the means of the microcanonical and Page distributions are in close agreement, we find that $P_{\mathrm{E}}(S_A)$ converges with increasing L to a *wider* distribution than Page, i.e., with a larger standard deviation. Both the right and left tails of $P_{\mathrm{E}}(S_A)$ contribute to the increased width; thus, in comparison to the Page distribution over random states, it is more likely for the entropy of FRC eigenstates to show larger positive *and* negative deviations from the Page mean.

In Fig. 2(b), we compare the first two moments of the Page and microcanonical distributions. We find that $\mu_P > \mu_U$, but the difference $(\mu_P - \mu_U)$ converges to zero exponentially with L. First, we normalize $(\mu_P - \mu_U)$ by $\mu_P \sim L$ and notice the exponential decrease in $(\mu_P - \mu_U)/\mu_P$ with increasing L. Next, even upon normalizing by $\sigma_P \sim \sqrt{2^{-L}}$, which is itself exponentially decreasing with L, we notice that not only is $(\mu_P - \mu_U)$ an order or magnitude smaller than σ_P, but the ratio $(\mu_P - \mu_U)/\sigma_P$ still shows a weak decrease with increasing L (consistent with plateauing at larger L). In contrast, the differences in standard deviations is more stark: The ratio of standard deviations σ_U/σ_P plateaus to a constant value of about 1.2, so the microcanonical standard deviation is about 20% larger than the Page standard deviation. In other words, while $\sigma_U \sim \sqrt{2^{-L}}$ shows the same exponential scaling as σ_P, the prefactor for the scaling is about 20% larger.

The different moments (normalized by σ_P) contribute to D_{KL} according to Eq. (4). We show in Fig. 2(c) that $D_{KL}^{(2)}$, the contribution from the second moment, is more than an order of magnitude larger than $D_{KL}^{(1)}$, the contribution from the first moment. In other words, while the average entropy of eigenstates of FRCs is well described by the average entropy of random pure states, the fluctuations of the microcanonical distribution are markedly larger, so an increase in the standard deviation is the dominant source of difference between the microcanonical and Page distributions. Since the FRC lacks any structure beyond locality, we attribute the relative increase in the standard deviation of $P_E(S_A)$ as a correction to RMT that arises from locality. [63] Indeed, in Appendix C, we show increasing convergence to the Page moments as the constraint of locality is relaxed by increasing the period of the Floquet circuit (i.e., by incorporating increasing numbers of even-odd layers). We obtain similar results by increasing the gate range while keeping the period fixed (Appendix C).

There are (at least) two mechanisms by which locality could affect entropy fluctuations. First, the entanglement entropy of eigenstates of local FRCs will be sensitive to the entangling properties of the local unitary gates straddling the entanglement cuts (in our case, these are two two-site gates displaced by half the system size). These local unitary gates have a much larger likelihood of being either weakly entangling (i.e., close to the identity) or maximally entangling (for example, close to the iSWAP gate) in comparison to global Haar random unitaries. Thus, even though the microcanonical distribution of entropy for local FRCs shows the same exponential scaling as for global Haar random circuits, $\sigma_U \sim \sqrt{2^{-L}}$, the effect of locality (and, in particular, the distribution in entangling power for local gates) could contribute to a larger prefactor for σ_U. This idea suggests that exploring different families of local FRCs could allow us to tune σ_U and D_{KL} to identify "maximally chaotic" families of circuits where D_{KL} is

minimized, which would be an eigenstate analog of the property of maximally chaotic dual-unitary circuits for which the Thouless time in the spectral form factor is minimized (and system-size independent) despite spatial locality [13]. We defer this analysis to future work.

Second, Refs. [18,42–44] showed that there are microcanonical correlations between expectation values of local operators computed in eigenstates of local Floquet circuits (also implying correlations between reduced density matrices of eigenstates, which are used to compute entanglement entropy as well). These correlations are not present in an RMT description of the system, and they arise from the presence of light cones in the spreading of local operators (or scrambling of quantum information) in spatially local systems. In particular, these correlations will be present even in dual-unitary models for which the Thouless time is minimized and agrees with RMT. While this analysis does not directly apply to the microcanonical distribution of half-system von Neumann entanglement entropy, it is reasonable to expect that eigenstate correlations of reduced density matrices could also affect the eigenstate entropy distribution. Understanding this connection better, and teasing apart different effects induced by locality that may contribute to increased σ_U, is also an interesting direction for future work.

In summary, the results of this section corroborate that D_{KL}, particularly microcanonical entropy fluctuations, furnishes a sensitive and easy-to-characterize metric for quantifying chaos via deviations from RMT. This metric can be used to compare different models with ease and can encapsulate various different effects of locality that may individually be more difficult to calculate, benchmark, and compare across models and observables. We now turn to studying this metric in a family of mixed-field Ising Hamiltonians parametrized by the strength of a transverse and longitudinal field. We will identify maximally chaotic models within this family of Hamiltonians by minimizing D_{KL} in parameter space.

IV. HAMILTONIAN SYSTEMS

We now consider the microcanonical distribution of EE produced by midspectrum eigenstates in the MFIM, a paradigmatic model that exhibits both chaotic and integrable limits depending on the model parameters. We first present the Bianchi-Dona distribution and argue why it serves as a better reference random distribution (as compared to the Page distribution) for Hamiltonian systems with energy conservation. We then introduce the MFIM model, generate the empirical distribution of midspectrum eigenstate entropies, $P_E(S_A)$, and compare the first two moments with the BD distribution. We quantify the distance between the distributions using the KL divergence, Eq. (4), and compare with conventional measures of quantum chaos such as level statistics.

A. Reference distribution II: Bianchi-Dona distribution

The presence of symmetries can affect the distribution of the EE. We argue that the symmetry of primary interest in this work corresponds to the conservation of an additive local scalar charge M. We refer to the distribution of entanglement entropy for pure random states subject to this constraint as the BD distribution [31], but note that some aspects of this ensemble of random states were previously discussed by Huang in Refs. [35,36]. We first describe this distribution and then argue why it captures important contributions of energy conservation to the EE of mid-spectrum eigenstates of spatially local Hamiltonians.

BD considered systems with an additive local charge that decomposes between a bipartition of the system into subsystems A and B as $M = M_A + M_B$. For concreteness, it is convenient to think of $0 \leq M \leq L$ as an integer particle number, with each site only able to accommodate a maximum of one particle. The Hilbert space $\mathcal{H}(M)$ of states with fixed charge M no longer has a tensor product structure but instead decomposes as a direct sum of tensor products:

$$\mathcal{H}(M) = \bigoplus_{M_A = \max(0, M - L_B)}^{\min(M, L_A)} \mathcal{H}_A(M_A) \otimes \mathcal{H}_B(M - M_A). \quad (11)$$

The Hilbert space dimension of $\mathcal{H}_A(M_A)$ is $d_{A,M_A} = \binom{L_A}{M_A}$, and the Hilbert space dimension of $\mathcal{H}_B(M - M_A)$ is $d_{B,M-M_A} = \binom{L - L_A}{M - M_A}$. The total Hilbert space dimension is $\sum_{M_A} d_{A,M_A} d_{B,M-M_A} = d_M = \binom{L}{M}$. A random state with fixed total charge $|\Psi_M\rangle \in \mathcal{H}(M)$ can be expressed as a superposition of orthonormal basis states,

$$|\Psi_M\rangle = \sum_{M_A} \sum_{\alpha=1}^{d_{A,M_A}} \sum_{\beta=1}^{d_{B,M-M_A}} \psi_{\alpha,\beta}^{(M_A)} |\alpha, M_A\rangle \otimes |\beta, M - M_A\rangle, \quad (12)$$

where the limits of the sum over M_A are the same as in Eq. (11), and $\psi_{\alpha,\beta}^{(M_A)}$ are uncorrelated random numbers up to normalization.

The reduced density matrix of such a state in subsystem A is of block-diagonal form, $\rho_{A,M} = \sum_{M_A} p_{M_A} \rho_{A,M_A}$, where the factors $p_{M_A} \geq 0$ come from normalizing ρ_{A,M_A} in each M_A sector and satisfy $\sum_{M_A} p_{M_A} = 1$. The probability of finding M_A particles in A is given by p_{M_A}, which is thus interpreted as the (classical) probability distribution of particle number in A. The entanglement entropy can then be expressed as

$$S(\rho_{A,M}) = \sum_{M_A} p_{M_A} S(\rho_{A,M_A}) - p_{M_A} \log p_{M_A}, \quad (13)$$

where the second term on the rhs is the Shannon entropy of the number distribution p_{M_A}, which captures particle number correlations between the two halves, while the first term captures quantum correlations between configurations with a fixed particle number [64].

The uniform measure on $\mathcal{H}(M)$ was derived in Ref. [31] and is the product of the distribution on the p_{M_A}'s and the uniform Haar measure within each number sector. The resulting analytical expression for the first two moments of the EE distribution for random states of the form Eq. (12) is reproduced in Appendix A (as a function of L, M), and these exact results are used in our numerical comparison below. In this section, we again discuss these moments in the limits $L_A, L_B \gg 1$, for which asymptotic forms were derived in Ref. [28]. In these limits, the average entanglement entropy of the BD distribution is given by

$$\mu_{\text{BD}}(f, m) \approx fL[-(1 - m)\log(1 - m) - m\log(m)]$$
$$- \sqrt{L}\delta_{f,1/2}\sqrt{\frac{m(1-m)}{2\pi}}\left|\log\left(\frac{1-m}{m}\right)\right|$$
$$+ \frac{f + \log(1 - f)}{2} - \frac{1}{2}\delta_{f,1/2}\delta_{m,1/2}, \quad (14)$$

where $m = M/L$. The first term is the volume law term that scales proportionately with $L_A = fL$, and the prefactor accounts for the reduced Hilbert space dimension in symmetry sector M. When $f = 1/2$, the EE has an additional $\sqrt{L}$ contribution, which comes from a saddle-point evaluation of the probability distribution of m and which has also been discussed in Refs. [26,27]. This correction can make finite-size analysis more complicated, but it vanishes at half-filling, $m = 1/2$, which is the maximum entropy case that will be of interest to us in our comparisons with infinite-temperature eigenstates.

Evaluating Eq. (14) at half-filling ($m = 1/2$) and for equal bipartitions ($f = 1/2$) yields

$$\mu_{\text{BD}}(f = 1/2, m = 1/2) \approx fL\log(2) - \frac{1}{2} + \frac{0.5 + \log(0.5)}{2}. \quad (15)$$

Relative to the Page entropy at $f = 1/2$, Eq. (6), this expression has an "extra" deficit of size $|0.5 + \log(0.5)/2| \approx 0.0966$ (see relative shifts in Page and BD distributions plotted in Fig. 1; numerical values for μ_P and μ_{BD} showing the 0.1 difference for $L = 8$ to 16 are shown in Table I of Appendix A). As we will show in the next section, this shift accounts for the $O(1)$ deviations between infinite-temperature eigenstates of local Hamiltonians (without any additional symmetries) and the Page entropy, which have been previously noted in the literature [34–36].

The second moment of the BD distribution in the $L_A, L_B \gg 1$ limit is approximated by

$$\sigma_{\text{BD}}^2(f, n) \approx \alpha L^{3/2} e^{-\beta L}, \quad (16)$$

where $\beta = -m \log m - (1-m) \log(1-m)$ and α is an $O(1)$ numerical prefactor in the limits of interest. At $m = f = 1/2$, the variances for the Page and BD distributions scale similarly with system size, i.e., around $1/d_B^2 \sim 2^{-L}$. Away from this limit, the rate of exponential decrease β is different for the two distributions. However, similarly to Page, $\sigma_{\mathrm{BD}}/\mu_{\mathrm{BD}} \ll 1$, so the average entropy of a constrained pure state in a fixed M sector is also typical.

Finally, note that we compare the BD distribution to the EE distribution produced by eigenstates of the MFIM model in Eq. (18). The MFIM has time-reversal symmetry, and thus its eigenstates are real-valued vectors, whereas the BD distribution was derived for complex random states. Thus, the references μ_{BD} and σ_{BD} need to be adjusted. For the case of unconstrained random states (i.e., without any symmetry), it has been found [61,65,66] that the distribution of EE for both real and imaginary pure random states asymptotically has the same mean value, given by the Page mean, $\mu_P^{\mathrm{GOE}} \approx \mu_P^{\mathrm{GUE}}$, Eq. (A3). On the other hand, the standard deviation of the EE distribution, σ_P, is (asymptotically) larger by a factor of $\sqrt{2}$ for real random states [61,65,66], $\sigma_P^{\mathrm{GOE}} \approx \sqrt{2}\sigma_P^{\mathrm{GUE}}$, where GOE and GUE refer to the orthogonal and unitary ensembles applicable for real and complex random states. The exact finite-size expressions for the mean and standard deviation of the EE of real random states look significantly more complicated than the expressions for the Page distribution for complex random states, but we show in Appendix A that numerically obtained values for the mean and standard deviation of real random states converge to μ_P^{GUE} and $\sqrt{2}\sigma_P^{\mathrm{GUE}}$ with increasing L. For constrained states, exact analytic results for real random states with charge conservation, i.e., the GOE version of the BD distribution, have not yet been derived. However, similar to the Page case, in Appendix A, we numerically find that the means of the EE distribution produced by real and imaginary states in a given symmetry sector converge to the same value with increasing L, while the standard deviation is again a factor of $\sqrt{2}$ larger for real states. In what follows, whenever we refer to σ_{BD}, we are referring to $\sigma_{\mathrm{BD}}^{\mathrm{GOE}}$, which is inflated by a factor $\sqrt{2}$ relative to the exact expression for σ_{BD} in Eq. (A6), while we continue to use the expression for μ_{BD} in Eq. (A5) for the mean [67].

1. Application of the BD distribution to midspectrum Hamiltonian eigenstates

We have seen in the previous section that the approach to compare the eigenstates of FRCs with unconstrained pure random states captures certain properties like the average entropy, while deviations from RMT due to locality are dominantly reflected in higher moments.

To generalize this analysis to Hamiltonian systems, we must contend with the fact that energy conservation adds additional structure that is not captured by the Page distribution and that already results in finite deviations in the average half-system entropy of infinite-temperature eigenstates [34–37] (see Fig. 1). The goal is to identify a new (more constrained) random state distribution that incorporates the effect of energy conservation so that differences between the new reference distribution and the microcanonical distribution can be dominantly attributed to features such as locality.

We now argue why the BD distribution furnishes a better RMT ensemble for describing midspectrum eigenstates of local Hamiltonians, even in the absence of additional $U(1)$ symmetries like particle number. The effect of energy conservation alone can be captured, within certain approximations, by that of conservation of a local additive $U(1)$ charge, and the BD distribution incorporates this feature. Our arguments recapitulate and build on part of the discussion in Ref. [36], which argued for an $O(1)$ deviation between the Page entropy and mean EE of Hamiltonian eigenstates.

As mentioned, we are interested in the eigenstate entanglement entropy S_A of a subsystem of size A. We write the Hamiltonian as $H = H_A + H_B + H_{AB}$, where H_A (H_B) has support in A (B) only and H_{AB} has support in both A and B. We can write any eigenstate of H with energy E, $|\psi_E\rangle$, in the basis of tensor products of eigenstates of H_A, H_B:

$$|\psi_E\rangle = \sum_{ij} c_{ij}|\epsilon_i\rangle_{\mathrm{A}}|\epsilon_j\rangle_{\mathrm{B}} \qquad (17)$$

Deutsch proposed [1] that Hamiltonian eigenstates could be modeled as random states in which c_{ij} is a random matrix with a narrow bandwidth that approximately imposes that the sum of energies of the subsystems is approximately equal to E: $\delta E_{ij} \equiv \epsilon_i + \epsilon_j - E \approx 0$ (the equality is not exact because of H_{AB}). Reference [27] used ETH to refine this conjecture to a more explicit form in which c_{ij} is modulated by a "window function" $F(\delta E_{ij})$ that penalizes deviations away from $\delta E = 0$ on a scale set by $\Delta = \sqrt{\langle \psi_E | H_{AB} | \psi_E \rangle}$.

With the condition $\delta E_{ij} \approx 0$, Eqs. (12) and (17) are conceptually very similar. However, there are also differences that we must treat with caution: (i) The presence of the H_{AB} term (which is also responsible for the state being entangled in the first place) means that the δE_{ij} is only approximately (rather than exactly) equal to 0. (ii) The spectrum of H is dense, so the Hilbert space does not factor into a sum of tensor products as in Eq. (13).

Both these differences can be addressed if we make an approximation that sets the window function $F(\delta E_{ij})$ to be strictly zero outside some width δ set by Δ so that c_{ij} is a strictly banded random matrix. This method is also well motivated because of a mathematical proof in Ref. [68], which shows that, for local Hamiltonians, there exist constants $c, \delta > 0$ such that $\sum_{\Delta E \geq \Lambda} |c_{ij}|^2 < c e^{-\Lambda/\delta}$.

The truncated state can now be put in the form of Eq. (12) [note that $\psi_{\alpha,\beta}^{M_A}$ in Eq. (12) is a banded random matrix] because the *same* truncated state can be equivalently obtained by discretizing the spectrum of H_A, H_B in steps of size δ so that all eigenvalues with energy $E_i - \delta/2 \leq E < E_i + \delta/2$ are assigned to the ith step E_i. This process produces a degeneracy for E_i, similar to the degeneracy in $M_{A/B}$ for the $U(1)$ case. Then, the truncated state is just a random constrained state with the *strict* constraint that $E_i + E_j = E$, which now looks identical to the $U(1)$ constrained state of the previous section in which the step size was 1. Thus, the Hilbert space is factored into a sum of tensor products, as in Eq. (13). The relative dimensions of the steps at different energies also become equivalent to the $U(1)$ case in the large system limit since the density of states of the Hamiltonian approaches a Gaussian, as does the binomial "choose" function, which sets the sizes of the $U(1)$ sectors.

We emphasize that the locality of the Hamiltonian is crucial for making the connection between the eigenstate and BD distributions. The truncation scale Δ is set by H_{AB}, and we need $\Delta \sim O(1)$ for the arguments above. More colloquially, we want H_{AB} to be a weak boundary term, which is necessary to couple the subsystems but can be taken to be arbitrarily small while still obtaining a thermal state. In contrast, we expect that eigenstates of long-range or k-local models (i.e., SYK models or systems with power-law interactions) will have the same universal properties as pure random states without any constraints, and we defer a more detailed analysis of this to future work.

Finally, we note that our arguments above do not rule out the possibility of nonuniversal $O(1)$ corrections in the mean EE induced by the truncation of the c_{ij} matrix and the presence of the H_{AB} term. Nevertheless, we find below that the agreement between BD and the Hamiltonian eigenstate distribution is surprisingly good and that it captures most of the observed difference between the eigenstate EE and Page mean. For this reason, we conjecture that the BD distribution is the best *universal* distribution to incorporate the effects of energy conservation.

B. Mixed-field Ising model

We now describe the Hamiltonian model studied in this work, the one-dimensional MFIM:

$$H = \sum_i (\sigma_i^z \sigma_{i+1}^z + g\sigma_i^x + h\sigma_i^z), \qquad (18)$$

where σ_i^α ($\alpha = x, y, z$) are Pauli matrices, g is the transverse field, and h is the longitudinal field. We use open boundary conditions in order to break translational symmetry, and we add additional boundary fields $h_1 = 0.25$ and $h_L = -0.25$ at the edges to break inversion symmetry. [69] The MFIM has various limits of physical interest. When $h = 0$, the model can be mapped to a free fermion model through a Jordan-Wigner transformation [70]; therefore, the model is noninteracting and integrable. A finite value of h breaks integrability. In addition, the model hosts two classical integrable limits: (i) $g = 0$ corresponds to the classical Ising model (diagonal in the σ^z basis), and (ii) $g \gg 1$ corresponds to the classical paramagnet (diagonal in the σ^x basis).

The MFIM has been extensively studied numerically in the context of thermalization and chaos [49,71,72], with diagnostics ranging from eigenstate entanglement entropy to level spacing ratio [71] to entanglement growth [49] and operator spreading dynamics [72,73]. These numerical studies have largely worked with two parameter choices that have been identified as showing particularly strong thermalizing behavior even at relatively small sizes: the Banuls-Cirac-Hastings (BCH) parameters [48], $g = -1.05$ and $h = 0.5$; and the Kim-Huse (KH) parameters [49], $g = (\sqrt{5} + 5)/8 \approx 0.9045$ and $h = (\sqrt{5} + 1)/4 \approx 0.8090$. These choices have become standard in the literature, and we will refer back to them once we discuss our numerical results. In particular, we find that these points are *not* the most chaotic with respect to the more resolved metric of chaos we present, even as various other standard diagnostics look chaotic at these parameter values.

In what follows, we focus on the distribution of entanglement entropy of midspectrum eigenstates for a half subsystem, $f = 1/2$, centered in the middle of the system. We use exact diagonalization to obtain the entire spectrum for system sizes up to $L = 14$ and fit the density of states (DOS) to find the energy corresponding to the peak of the DOS, i.e., to infinite temperature [since $\text{Tr}(H) = 0$, the value of energy corresponding to infinite temperature approaches zero with increasing size, but finite-size systems can show small deviations within the scale of energy fluctuations]. We then obtain the EE of all eigenstates centered in a small energy window around the peak energy and compute the mean and standard deviation of the EE of these eigenstates, denoted μ_H and σ_H, respectively. Here, the subscript H refers to "Hamiltonian," to be contrasted with Floquet unitaries studied in the previous section, and is thus more descriptive than the μ_E and σ_E symbols introduced in Sec. II, which referred collectively to eigenstate distributions of either Hamiltonian or Floquet systems.

The number of eigenstates within the energy window centered at the DOS peak is chosen large enough to minimize the uncertainty of μ_H and σ_H but small enough to avoid systematic effects induced by finite-temperature eigenstates. Here, we use windows with 100, 400, and 600 states for $L = 10$, $L = 12$, and $L = 14$, respectively. For larger system sizes ($L = 16$), we do not diagonalize the full spectrum but, instead, use the shift-invert method [58] to find 2000 eigenstates closest to $E = 0$. Our results are quite robust to changes in the number of states chosen, and a discussion on selecting a window size with an appropriate number of states is presented in Appendix B.

For comparison, we also show data for the level spacing ratio [12] averaged over the same energy windows defined above. The ratio factor is a commonly used diagnostic of level repulsion and is defined using three consecutive eigenstates, $\{E_{n-1}, E_n, E_{n+1}\}$, as

$$0 \leq r_n = \frac{\min(\Delta E_n, \Delta E_{n+1})}{\max(\Delta E_n, \Delta E_{n+1})} \leq 1, \qquad (19)$$

with $\Delta E_n = E_n - E_{n-1}$. Integrable systems exhibit uncorrelated level statistics described by a Poisson distribution with average ratio factor $\langle r \rangle = 0.386$ [10]. Chaotic systems exhibit level repulsion described by Wigner-Dyson statistics with an average ratio factor $\langle r \rangle = 0.536$ [10].

C. First moment of the EE distribution

We begin our discussion by focusing only on the first moment of the microcanonical EE distribution μ_H, and we study its system-size dependence. Figure 3 shows μ_H as a function of the transverse field g while keeping h fixed to $h = 0.3$. The choice of $h = 0.3$ corresponds to a strongly chaotic cut, as will become clear in the next subsection. All curves are normalized by the theoretical value of the first moment of the BD distribution, μ_{BD}, obtained from Eq. (A5) of Appendix A and evaluated at half-filling (maximum entropy), $m = 1/2$, and equal bipartition, $f = 1/2$.
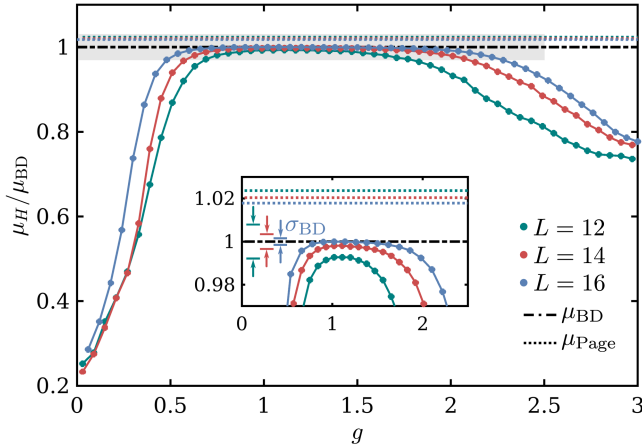

FIG. 3. Finite-size scaling of the first moment μ_H of the microcanonical entanglement entropy distribution of Hamiltonian eigenstates plotted as a function of the transverse field g in the MFIM. Results are normalized with respect to the first moment μ_{BD} of the BD distribution. Curves are plotted for system sizes $L = 12$, 14, and 16 and a longitudinal field $h = 0.3$. We see that the microcanonical mean converges to μ_{BD}. The inset is a zoomed version of the main panel (see shaded region) showing the approach to the BD distribution (dotted dashed lines) and statistically significant deviations from the Page distribution (dotted lines). The arrows indicate the standard deviation σ_{BD} of the BD distribution for the different system sizes.

We find excellent agreement between the means μ_H and μ_{BD} in a wide range of parameters centered around $g \approx 1.1$. In particular, for $L = 16$, we find agreement between μ_H and μ_{BD} up to the fifth significant digit. In addition, by increasing the system size, we observe that μ_H approaches μ_{BD} in an increasingly larger region of parameter space: Although there are sizable deviations between μ_H and μ_{BD} close to integrable limits ($g \ll 1$ or $g \gg 1$), they tend to decrease with increasing system size. To leading order, this behavior agrees with that observed using spectral metrics of chaos: The MFIM exhibits chaotic behavior for all finite values of g in the thermodynamic limit.

In contrast, we observe statistically significant deviations between μ_H and the mean EE of pure random states without any constraint μ_P (dotted lines) for *all* values in parameter space and for all system sizes, consistent with recent observations [34–36]. Such behavior is visible in the inset of Fig. 3, which shows a zoomed version of the main panel with μ_P, Eq. (A3), plotted with dotted lines. These results provide strong numerical corroboration that, in contrast to the Page distribution, the BD distribution is a better reference RMT distribution for midspectrum eigenstates of local Hamiltonians.

At the level of the first moments, the Hamiltonian results are analogous to the FRC results: Pure random states (with appropriate constraints) correctly describe the first moment of the EE distribution of eigenstates in quantum chaotic systems. In the following two subsections, we use the more refined metric D_{KL}, which compares differences on the exponentially small scale set by σ_R and also incorporates the effects of the second moment of the EE distributions.

D. Kullback-Liebler divergence and maximally chaotic Hamiltonians

Having discussed the behavior of the first moment of the microcanonical EE distribution relative to the BD distribution, we now employ our more refined measure of "distance between distributions" using the KL divergence. As discussed in Sec. II, we only use the first two moments to compute the KL divergence via Eq. (4).

Figure 4(a) shows the value of D_{KL} as a function of model parameters (g, h) for $L = 14$. A noticeable feature of Fig. 4(a) is that, for most of the parameter space, the eigenstate and RMT distributions exhibit relatively large deviations from each other. Indeed, there is only a small region of parameter space where the value of D_{KL} is small (i.e., $D_{\mathrm{KL}} \lesssim 1$). The minimum value for D_{KL} is obtained for $(g_*, h_*) = (1.10 \pm 0.05, 0.30 \pm 0.05)$, which thus corresponds to the MC parameters for this metric and this family of MFIM Hamiltonians. The KL divergence increases exponentially as (g, h) are tuned away from the MC parameters, Fig. 4(c). The MC parameters that we find are relatively close to the BCH parameters in Ref. [48] but far from the KH parameters in Ref. [49], even though both sets of parameter choices are widely employed
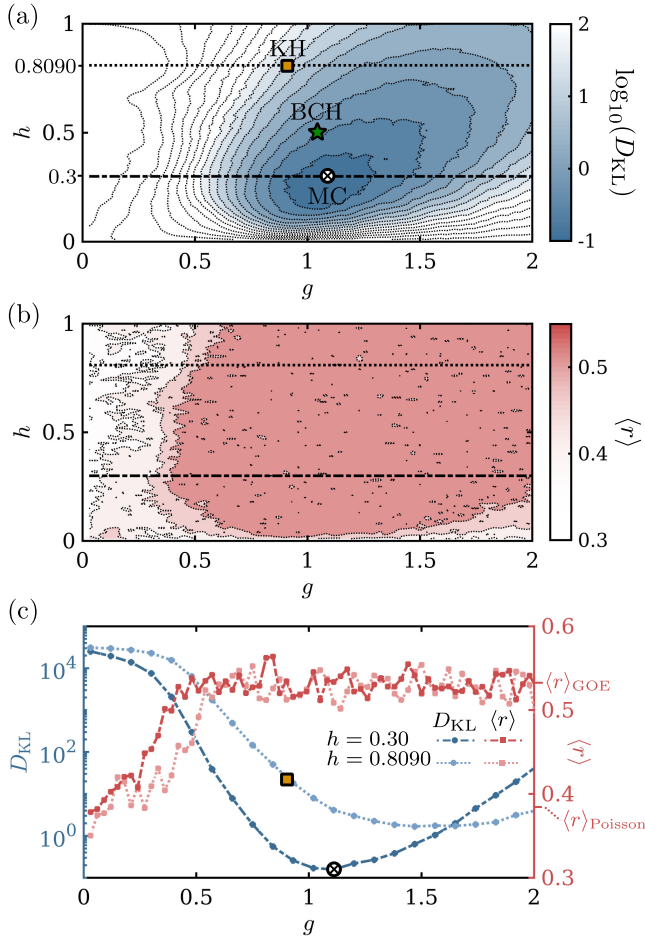
FIG. 4. Color maps of (a) the KL divergence and (b) the average ratio factor $\langle r \rangle$ computed for the MFIM with transverse field g and longitudinal field h, for $L = 14$. The D_{KL} contour plot shows that, within the parameter space of the MFIM model, the parameter values near $(g_*, h_*) = (1.1 \pm 0.05, 0.30 \pm 0.05)$ are the most chaotic, with D_{KL} steeply increasing away from these values. Also indicated are the KH (square) and BCH (star) parameters that have been widely used in studies of thermalization, which show much larger values of D_{KL}. In contrast, panel (b) shows that the value of $\langle r \rangle$ is saturated at the RMT value, signals chaos in a broad region of parameter space (including the BCH and KH parameters), and does not exhibit the resolution observed in panel (a). (c) Horizontal linecuts of D_{KL} and $\langle r \rangle$ across the MC and KH parameters; see horizontal dotted-dashed and dotted lines, respectively, in panels (a) and (b). The reference GOE and Poisson ratio factors are indicated on the right vertical axis.

in studies of chaos in the MFIM. Both parameter choices are indicated in Fig. 4(a). In the next subsection and in Appendix E, we show a more detailed comparison between the MC parameters identified in this work and those commonly used in the literature.

To contrast the behavior of D_{KL} with other metrics of chaos, in Fig. 4(b), we plot the average level spacing ratio $\langle r \rangle$ as a function of g and h. We find that $\langle r \rangle$ is featureless

and saturates to the RMT value $\langle r \rangle \approx 0.54$ in a very broad region of parameter space, unlike D_{KL}, which is only minimized in a small region of parameter space around $(g_*, h_*) = (1.1, 0.35)$. Figure 4(c) shows two linecuts as a function of g, at the h value corresponding to the MC and KH points. We see that $\langle r \rangle$ quickly saturates to the RMT value away from the $g = 0$, while D_{KL} shows strong variation in parameter space even for parameters for which $\langle r \rangle$ looks strongly chaotic. This finding is consistent with the general picture discussed above, which argues that D_{KL} is a much more resolved metric of quantum chaos.

The enhanced proximity to RMT behavior in a small pocket of parameter space is quite striking: It seems to indicate that maximally chaotic local Hamiltonians—those with microcanonical distributions of EE reproducing the first and higher moments of pure random state distributions—are not typical. Although our two-parameter model exhibits agreement with RMT in a small region of parameter space, a tantalizing possibility is that these small regions shrink to a fine-tuned point when extending the space of local Hamiltonian models to include a larger number of parameters. This idea is reminiscent of integrable models that are assumed to be fined-tuned points in parameter space. It is also reminiscent of special classes of Floquet models, namely, dual-unitary Floquet models, in which the spectral form factor shows a Thouless time equal to 1 and which are therefore considered maximally chaotic from the lens of spectral statistics [13]. While our analysis is restricted to the two-dimensional parameter space of the MFIM, an interesting question for future study is whether there exists a Hamiltonian with more parameters (but still local) where the distance to RMT behavior is provably minimal.

Finally, as commented above, we emphasize that these results—the excellent agreement between the EE behavior of eigenstates and constrained RMT ensembles in small pockets of parameter space—are insensitive to the choice of entanglement observable used. In Appendix F, we reproduce these results by using, instead, the second Renyi entropy S_2.

E. Higher moments of the EE distribution

We finish our discussion of Hamiltonian systems by showing the full EE distribution of midspectrum eigenstates for various representative parameter values and parsing how different moments of the microcanonical EE distribution contribute to D_{KL} for different linecuts.

Figure 5 shows (a) $|\mu_H - \mu_{\mathrm{BD}}|/\sigma_{\mathrm{BD}}$ and (b) $\sigma_H/\sigma_{\mathrm{BD}} - 1$ for $h = (1 + \sqrt{5}/4) \approx 0.8090$ (the Kim-Huse choice) and as a function of g. Both ratios are normalized with σ_{BD}, as they appear in the definition of D_{KL}. We observe substantial variation in these ratios as a function of g, with both quantities (and hence D_{KL}) changing by orders of magnitude as g is tuned. The moments are closest to the BD predictions near $g \approx 1.5$. Interestingly, we observe a good
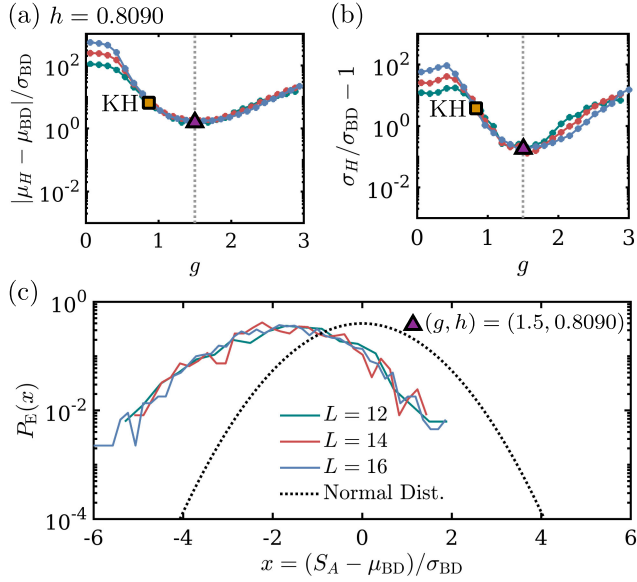
FIG. 5. (a) Difference between the EE mean of midspectrum eigenstates and μ_{BD} normalized with the EE standard deviation of pure random states. (b) Ratio between the EE standard deviation of midspectrum eigenstates and σ_{BD} as a function of system size and transverse field g. Plots are shown for $L = 12$, 14, and 16, and for $h = (1 + \sqrt{5})/4 \approx 0.8090$. The number of states used to compute the first two moments is discussed in the main text. The vertical dashed line indicates the most chaotic point (minimal D_{KL}) along this linecut ($g \approx 1.5$), while the square symbol indicates the KH parameters. (c) Histogram of midspectrum entanglement entropy for the most chaotic point along this linecut, $(g, h) = (1.5, 0.8090\ldots)$, as a function of system size. The reference standard normal distribution is shown with dotted lines.

collapse of both ratios as a function of L in the parameter region $1 \lesssim g \lesssim 2$ centered around $g \approx 1.5$. In other words, in this regime, both the microcanonical and RMT standard deviations scale similarly with system size, $\sigma_H \sim \sigma_{\mathrm{BD}} \sim \sqrt{2^{-L}}$, but, similar to the Floquet case, σ_H still has a systematically larger prefactor by about 20%. Likewise, the difference between the means is exponentially small in L, again with the same scaling as σ_{BD}. In this chaotic (but not maximally chaotic) regime, the value of D_{KL} appears to converge with L to a fixed value.

On tuning g away from the chaotic region near $g \approx 1.5$, we observe a crossover in the functional dependence of σ_H with L, which goes from displaying chaotic scaling [in particular, σ_H decreasing exponentially with increasing system size according to Eq. (16)] to near-integrable behavior (σ_H decreasing polynomially with increasing system size). Accordingly, the ratio $\sigma_H/\sigma_{\mathrm{BD}}$ increases exponentially with L near integrability (g small). Similarly, the ratio $|\mu_H - \mu_{\mathrm{BD}}|/\sigma_{\mathrm{BD}}$ increases exponentially with L in the same near-integrable regime, where the difference in microcanonical and BD means is only polynomially converged. Remarkably, we see that the sensitivity of the two ratios

shows deviations from RMT over a large range of g's, with the near-integrable scaling observed throughout the window $0 \le g \lesssim 0.8$ and persisting all the way to $g \sim 0.8$, which is comparable to J. These more sensitive metrics also reveal that the Kim-Huse parameter choice $g \approx 0.9$ (marked by a square in Fig. 5) is surprisingly near the crossover from the integrable to chaotic scaling in the ratios, in contrast to measures like $\langle r \rangle$ which look strongly chaotic for the KH parameters.

We note that previous works have employed the crossover from power-law to exponential scaling of the fluctuations of local operators as a way to distinguish chaotic from integrable behavior [60]. This method was shown to be a more sensitive probe of chaos as compared to spectral metrics such as the ratio factor, in the sense of detecting chaos *before* the ratio factor when tuning away from an integrable point. In contrast, we use our ratios to detect deviations from chaos even in regimes where $\langle r \rangle$ looks strongly thermal.

In Fig. 5(c), we show the full distribution of EE of midspectrum eigenstates, appropriately shifted and rescaled, for $g = 1.5$, which is the most chaotic point with minimal D_{KL} along this linecut (denoted by a triangle in Fig. 5). The rescaled distributions appear to be well converged with system size. Compared to the FRC data in Fig. 2, we notice that the mean *also* shows a sizable departure and is several standard deviations away from σ_{BD}.

Indeed, in most of the parameter space away from the MC point marked in Fig. 4, we notice that the main contribution to D_{KL} comes from the first moment, although $D_{\mathrm{KL}}^{(1)}$ and $D_{\mathrm{KL}}^{(2)}$ closely track each other in their qualitative behavior as a function of g. Given this observed departure in the first moment, in Appendix D, we also present a related diagnostic of chaos which is agnostic to the reference RMT distribution and only looks at the (normalized) fluctuations of EE: $\sigma_H/\sqrt{2^{-L}}$. This ratio is expected to be system-size independent and minimized for maximally chaotic systems while being exponentially increasing for L for near-integrable systems. Figure 11 in Appendix D shows that this ratio yields a qualitatively similar landscape of chaos in parameter space as D_{KL} in Fig. 4(a).

Next, in Fig. 6, we plot the same ratios as in Fig. 5 but for a cut at $h = 0.3$, which includes the maximally chaotic point that minimizes D_{KL} in the (g, h) parameter space. Again, in the near-integrable regimes ($g \approx 0$ and $g \gg h$), the ratios involving both moments show an exponentially increasing trend with L, for reasons identical to those discussed above. There is, however, a notable difference from Fig. 5 in the parameter regime near the MC point at $g \approx 1.1$. In particular, we find that both ratios show a sharp change for the largest size ($L = 16$), showing much better convergence with the BD predictions at the MC point, and the ratio involving the first moment shows a steep increase away from the MC point, as shown in Fig. 6(a). In fact, we
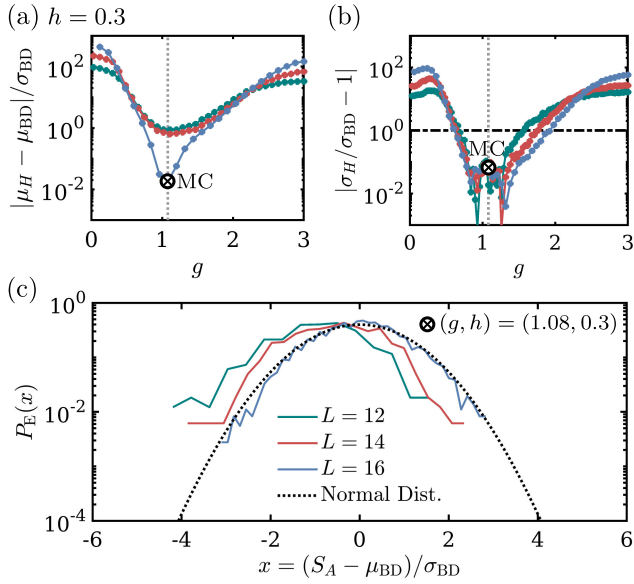
FIG. 6. (a) Difference between the EE mean of midspectrum eigenstates and μ_{BD} normalized by σ_{BD}, and (b) ratio between EE standard deviations of midspectrum eigenstates and σ_{BD} as a function of system size and transverse field g. Plots are shown for $L = 12$, 14, and 16, and for $h = 0.3$. The number of states used to compute the first two moments is discussed in the main text. The vertical dashed line indicates the most chaotic point (minimal D_{KL}) along this linecut ($g = 1.08$), which also coincides with the most chaotic parameters in the 2D parameter space. (c) Histogram of midspectrum EE for the most chaotic parameters as a function of system size, showing an approach to RMT behavior. The reference standard normal distribution is shown with dotted lines.

also observe that, for a small range of parameters near $g = 1.1$, the microcanonical standard deviation is even slightly smaller than the reference σ_{BD}, which is why we plot the absolute value of the deviation of this ratio from 1 in Fig. 6(b). The full distribution of midspectrum eigenstates for the MC parameters is shown in panel (c), showing almost perfect agreement with the BD distribution at $L = 16$, even more so than the FRC data in Fig. 2, which showed an observable difference in the second moment.

This near-perfect agreement with the BD distribution at the MC point and the sharp change in behavior with L and g near this point is quite surprising—a priori, one might expect deviations from BD everywhere in parameter space given that the Hamiltonian is local and only has two tuning parameters. One might also expect a gentler change in behavior in parameter space away from the MC point, contrary to what is observed in Fig. 6(a). We defer a more detailed analysis of the MC point and perturbations away from it to future work.

V. DISCUSSION AND OUTLOOK

We introduce a framework that allows us to quantify beyond-RMT correlations in quantum chaotic systems by comparing the ensemble properties of eigenstates and those of pure random states. In particular, our framework relies on introducing a quantitative notion of distance using the Kullback-Liebler divergence to compare the microcanonical distribution of EE generated by eigenstates of local Floquet or Hamiltonian systems and a reference random distribution. This notion of distance serves as a much more resolved measure of chaos than those conventionally used in the literature, such as level spacing statistics, as it compares higher moments of the microcanonical and reference distributions on the exponentially small scale set by σ_R. As a result, it not only distinguishes between integrable and chaotic behavior but also furnishes a continuous "ruler" that measures deviations from RMT even as other spectral metrics such as the level spacing ratio have saturated to their thermal values.

Besides introducing a new method for characterizing thermalization, we emphasize several other ramifications of our work. First, we show that the distribution of entanglement entropy deviates from RMT predictions even in paradigmatic models of strongly thermalizing dynamics, namely, FRCs without any structure other than locality. This case is primarily reflected in the ratio $\sigma_U/\sigma_P > 1$, which is larger than 1 and stable with increasing system size. An interesting direction for future work is to understand how different physical effects stemming from locality contribute to the increased standard deviation. For example, prior works [18,39–44] have shown that the existence of a light cone in the spreading of operators in local quantum systems leads to beyond-RMT spectral correlations in the eigenstate expectation values of local operators. It would be fruitful to try to establish a quantitative connection between these correlations and the increased standard deviation of the microcanonical ensemble. Locality also implies that the entangling properties of the local gates in the FRC (those that straddle the entanglement cut) play an important role in the eigenstate entanglement.

Second, our work provides evidence that a more suitable reference distribution for comparing eigenstates of local Hamiltonian systems is the Bianchi-Dona distribution [which accounts for the presence of a $U(1)$ charge] as opposed to the Page distribution, which has been the standard reference distribution in almost all previous works. In particular, building on Ref. [36], we argue that local Hamiltonians with energy conservation effectively have a local scalar charge that behaves similarly to the $U(1)$ charge for infinite-temperature eigenstates and for large enough subsystems. An important direction for future work is to better understand the effects of finite temperature, locality, and symmetries (including multiple, possibly noncommuting symmetries, or kinematic constraints like dipole-moment conservation or Rydberg blockades) in setting the appropriate reference RMT ensemble for Floquet or Hamiltonian systems and to try to incorporate the universal contributions of these features into the

reference distribution. Separate from the challenge of finding an appropriate reference distribution, we showed that the microcanonical fluctuations of EE (normalized by $\sqrt{2^{-L}}$) serve as an independent (and reference agnostic) diagnostic of chaos, which qualitatively displays similar behavior to D_{KL} in parameter space and is minimized for the most chaotic models.

Third, our results show a strong and surprising variation of D_{KL} in parameter space for the MFIM, showing strong deviations away from RMT even for parameters that have been previously identified as strongly chaotic and in parameter regimes where other metrics have saturated to chaotic values. Conversely, we observe that D_{KL} is minimized in small pockets of parameter space, suggesting that there might be families of maximally chaotic Hamiltonians. This case is somewhat reminiscent of "minimally chaotic" (integrable) systems, which are known to be fine-tuned points of measure zero in parameter space, or maximally chaotic dual-unitary Floquet circuits. More detailed studies about these maximally chaotic regions (or points) and understanding their dynamical properties remain open directions for future research.

Finally, our method relies on measuring the entanglement patterns of typical quantum states of physical systems, posing interesting challenges in the experimental implementation of our approach. Entanglement observables have traditionally been very hard to measure, as they require performing quantum state tomography on subsystem properties—a task that requires an exponentially large amount of measurements on the number of subsystem degrees of freedom. However, it has recently been noted that one can bypass quantum state tomography and access important properties of quantum states in an experimentally efficient way. One such approach is the "randomized measurement toolbox" [74], which gives access to properties such as the Renyi entropies [75,76], entanglement of mixed states [77], Fisher information [78], fidelities [79], the spectral form factor [80], and conservation laws [81], among others. In addition, while preparing individual eigenstates in experiments is extremely challenging, it is plausible that one can effectively sample the microcanonical ensemble from the late-time dynamics if the initial state is properly chosen. In the context of Hamiltonian systems, a suitable approach would be to use low-entanglement initial states (i.e., states that are easy to prepare using a few local operations) having small energy variance [82,83]. Using these modern capabilities to find the best pathway to diagnose and quantify quantum chaos in experiments is an interesting direction for future work.

ACKNOWLEDGMENTS

APPENDIX A: MOMENTS OF THE ENTANGLEMENT ENTROPY DISTRIBUTION FOR PURE RANDOM STATES

1. Page distribution for pure random states

The distribution of entanglement entropy averaged over pure random states was computed analytically in several works [31,61,62]. A pure state $|\psi\rangle$ on the composite system $\mathcal{H} = \mathcal{H}_A \otimes \mathcal{H}_B$ can be expanded as a linear combination

$$|\psi\rangle = \sum_{i=1}^{d_A} \sum_{j=1}^{d_B} C_{i,j}|i\rangle \otimes |j\rangle, \tag{A1}$$

where d_A (d_B) is the Hilbert space dimension of system A (B), and the coefficients $C_{i,j}$ are the entries of a rectangular $d_A \times d_B$ matrix C. The reduced density matrix for such a state after tracing out the degrees of freedom in system B is

$$\rho_A = \sum_{i,i'=1}^{d_A} W_{ii'}|i\rangle\langle i'|, \tag{A2}$$

with $W_{ii'} = \sum_j C_{ij}C_{i'j}^* = (CC^\dagger)_{ii'}$. The entanglement entropy $S(\rho_A) = \sum_i \lambda_i \ln \lambda_i$ for $|\Psi\rangle$ is determined from the spectrum $\{\lambda_i\}$ of W. For random states, the coefficients $C_{i,j}$ are independently and identically distributed real (GOE) or complex (GUE) Gaussian variables, following the distributions $P(C) \propto \exp\{-(\beta/2)\mathrm{Tr}(C^\dagger C)\}$, where $\beta = 1$ for the GOE ensemble and $\beta = 2$ for the GUE ensemble. In such cases, the product $W = CC^\dagger$ is known as a random Wishart matrix, and the joint probability distribution $P(\{\lambda_i\})$ has been well characterized [84], which allows one to compute all the moments of S_A for real and random state ensembles.

The statistical properties of *complex* random states, which are descriptive of eigenstates of FRC or systems with broken time-reversal symmetry (TRS), are better understood than those of *real* random states, which are descriptive of the eigenstates of the MFIM. We begin by presenting the exact formulas for the mean and standard deviation of the EE distribution for complex random states

($\beta = 2$). Then, we discuss how the asymptotic values are affected when the states are real ($\beta = 1$).

a. Moments of the GUE ($\beta = 2$)

As shown in Ref. [31], the first moment of the distribution $P(S_A)$ for complex random states in a qubit system of size L is given by

$$\mu_{\mathrm{P}} = \Psi(d_A d_B + 1) - \Psi(d_B + 1) - \frac{(d_A - 1)}{2d_B}, \quad (A3)$$

where $\Psi(x) = \Gamma'(x)/\Gamma(x)$ is the digamma function, defined as the logarithmic derivative of the Gamma function, and where $d_A = 2^{L_A}$ and $d_B = 2^{L-L_A}$ are the dimensions of the subsystems A and B. This expression can be evaluated exactly for all system and subsystem sizes. The asymptotic form of Eq. (A3) in the limit of $L \to \infty$ and $f = L_A/L$ is written in Eq. (6) of the main text. The variance of the entanglement entropy distribution $\sigma_{\mathrm{P}}^2 = \langle S_A^2 \rangle - \langle S_A \rangle^2$ is given by

$$\sigma_{\mathrm{P}}^2 = \frac{d_A + d_B}{d_A d_B + 1} \Psi'(d_B + 1) - \Psi'(d_A d_B + 1)$$
$$- \frac{(d_A - 1)(d_A + 2d_B - 1)}{4d_B^2(d_A d_B + 1)}. \quad (A4)$$

The asymptotic expression of Eq. (A4) in the limit of $L \to \infty$ and fixed $f = L_A/L$ is given in Eq. (8) of the main text. The numerical values for μ_{P} and σ_{P} for different system sizes are shown in Table I.

b. Moments of the GOE ($\beta = 1$)

Systems with TRS have a smaller effective Hilbert space dimension than those without TRS. Consequently, we expect the average entropy for real random states to be upper bounded by that of complex ones. While the exact expressions for the means differ, it was shown in Refs. [61,65,66] that they are asymptotically the same in the thermodynamic limit. However, the standard deviation acquires an additional $\sqrt{2}$ prefactor relative to the GUE ensemble, $\sigma_P^2(\beta = 1) \sim 2\sigma_P^2(\beta = 2)$, since the GUE ensemble averages over both the real and complex parts. This

TABLE I. Mean and standard deviation of the Page and Bianchi-Dona distributions as a function of system size for random complex states ($\beta = 2$) and $L_A = L/2$. For the BD distribution, we consider systems at half-filling, $m = M/L = 1/2$.

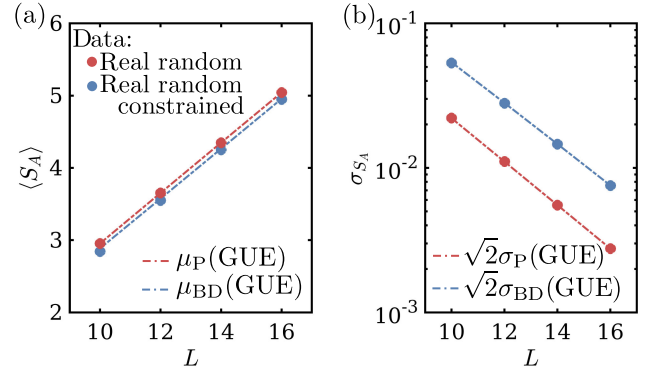| L	μ_{P}	σ_{P}	μ_{BD}	σ_{BD}
8	2.2749	0.0311	2.2062	0.0718
10	2.9663	0.0156	2.8866	0.0380
12	3.6590	0.0078	3.5745	0.0199
14	4.3521	0.0039	4.2652	0.0103
16	5.0452	0.0020	4.9569	0.0053

FIG. 7. (a) Numerical data for the mean entanglement entropy of real random states constrained to the $M = L/2$ symmetry sector (blue dots) and real random states in the full Hilbert space (red dots). The numerical data are obtained from 10^6 randomly generated states. For comparison, the analytic Page and BD means for the entanglement entropy distribution of random states with and without constraints are shown with dotted-dashed lines. (b) Numerical data for the standard deviations of the entanglement entropy using the same randomly generated data as in panel (a) (blue and red dots), compared against the analytic values of σ_{P} and σ_{BD} inflated by $\sqrt{2}$ to account for the larger standard deviation of real random states.

behavior is explicitly shown in Fig. 7, where the first two moments of $P_{\mathrm{R}}(S_A)$ are computed numerically by generating 10^6 real random states and compared against the asymptotic predictions, μ_P and $\sqrt{2}\sigma_P$.

2. Bianchi Dona for constrained random states

The presence of a $U(1)$ charge causes the reduced density matrix in Eq. (A2) to become block diagonal in the charge sectors. To analyze the statistical properties of such systems, we present the exact formulas for the first two moments of complex random states subject to an additive constraint, which were first derived in Ref. [31]. To the best of our knowledge, there are no known analytic results for constrained real states. However, based on numerical experiments, we show below that the conclusions of the unconstrained GOE ensemble translate to the constrained $U(1)$ scenario; namely, fluctuations are enhanced by a factor of $\sqrt{2}$ relative to the GUE ensemble, whereas the means agree in the thermodynamic limit.

a. Constrained GUE ensemble ($\beta = 2$)

When the pure complex random states are constrained to a given symmetry sector M, the first moment of the distribution is given by [31]

$$\mu_{\mathrm{BD}}(M) = \sum_{M_A = 0}^{M} \frac{d_{M_A}}{d_M} (\mu_{\mathrm{P}}(M_A) + \Psi(d_M + 1) - \Psi(d_{M_A} + 1)),$$
$$(A5)$$

where $\mu_{\mathrm{P}}(M_A)$ is the Page mean, Eqs. (A3), constrained to the subspace $\mathcal{H}_A(M_A) \otimes \mathcal{H}_B(M - M_A)$, which means that the effective subsystem Hilbert space dimensions are $d_{A,M_A} = \binom{L_A}{M_A}$, $d_{B,M-M_A} = \binom{L-L_A}{M-M_A}$, $d_{M_A} = d_{A,M_A} d_{B,M-M_A}$, and the total Hilbert space dimension is

$\sum_{M_A} d_{A,M_A} d_{B,M-M_A} = d_M = \binom{L}{M}$. The asymptotic form of Eq. (A5) in $L \to \infty$ for fixed $f = L_A/L$ and $m = M/L$ is given in Eq. (14) of the main text. The second moment of the entanglement entropy distribution for random states constrained to the M-symmetry sector is given by

$$\sigma_{\mathrm{BD}}^2 = \sum_{M_A} \frac{d_{M_A}(d_{M_A}+1)}{d_M(d_M+1)}((\sigma_{\mathrm{P}}^2(M_A) - \Psi'(d_M+2) + \Psi'(d_{M_A}+2) + (\mu_{\mathrm{P}}(M_A) + \Psi(d_M+2) - \Psi(d_{M_A}+2))^2)$$

$$+ \sum_{M_A' \neq M_A} \frac{d_{M_A} d_{M_A'}}{d_M(d_M+1)}((\mu_{\mathrm{P}}(M_A') + \Psi(d_M+2) - \Psi(d_{M_A'}+1))(\mu_{\mathrm{P}}(M_A) + \Psi(d_M+2) - \Psi(d_{M_A}+1)) - \Psi'(d_M+2)) - \mu_{\mathrm{BD}}^2,$$

(A6)

where $\sigma_{\mathrm{P}}^2(M_A)$ is the Page variance, Eq. (A4), constrained to the subspace $\mathcal{H}_A(M_A) \otimes \mathcal{H}_B(M - M_A)$. The numerical values of μ_{BD} and σ_{BD} for different system sizes are shown in Table I.

b. Constrained GOE ensemble ($\beta = 1$)

Eigenstates of systems with TRS are real valued; thus, it is necessary to extend Eqs. (A5) and (A6) for the case of real random states. We are not aware of any analytical results in this case. For this reason, we numerically compute the distribution of entanglement entropies of real random states constrained to the $M = L/2$ symmetry sector of a spin-1/2 chain. The moments are obtained by considering 10^6 samples for system sizes ranging from $L = 10$ to $L = 16$. As shown in Fig. 7, the mean of the EE distribution agrees with the analytic expression derived for complex states, whereas the standard deviation increases by a factor of $\sqrt{2}$. This behavior is analogous to the analytical results obtained for unconstrained Haar random states.

APPENDIX B: WINDOW SIZE DEPENDENCE OF THE EE MOMENTS

In the main text, we discussed the number of eigenstates used to compute the microcanonical mean and standard deviations for the Hamiltonian and Floquet models. Here, we present numerical evidence that our results are not sensitive to the choice of window size, as long as the window is sufficiently large to obtain reliable estimates of the moments and (for the Hamiltonian case) sufficiently small to avoid the effects of lower-temperature eigenstates.

1. Floquet random circuits

In Fig. 8, we show data for the mean and standard deviation of S_A for eigenstates of the FRC on $L = 12$ qubits as a function of window size N. For a given circuit realization, we divide the spectrum into groups of N states closest in quasienergy. We compute the mean and standard deviation in each window of size N, then average these

across the spectrum, and finally across circuit realizations. The first moment is independent of N at this resolution; we observe that only approximately 50 eigenstates of the FRC are necessary for the ratios involving the first two moments to converge. In our data, we use the full spectrum for $L \leq 14$ while we use windows of 50 states centered at different quasienergies for $L = 16$.

2. Mixed-field Ising model

When computing the microcanonical mean and variance of the distribution $P_H(S_A)$ for midspectrum energy density E eigenstates, it is necessary to use a finite window ΔE to take samples of S_A. In general, if ΔE is too small, then a statistically small number of states will be available for sampling, thus resulting in large error bars. On the other hand, if ΔE is too large, then low entanglement eigenstates will skew the distribution and increase its variance. Similarly to the FRC case, we argue that, because of typicality, only a few eigenstates are necessary to quantify the mean and standard deviation of the distribution. Here, we numerically show that this is the case. In particular, we show that the value of the standard deviation of S_A for midspectrum eigenstates does not vary appreciably when the window size is reasonably small; thus, the results
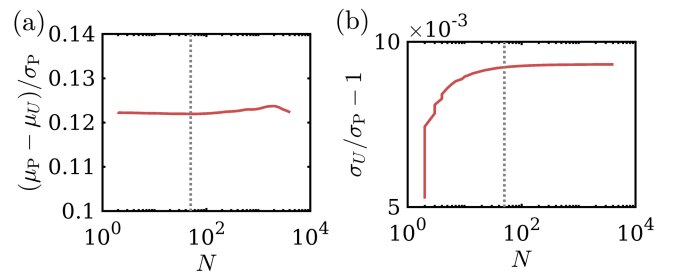

FIG. 8. Average (a) mean and (b) standard deviation of the EE as a function of window size. For each value of N, we average over different centers for the window and over 100 circuit realizations. The vertical dotted lines indicate the window of 50 eigenstates used in the data of the main text.
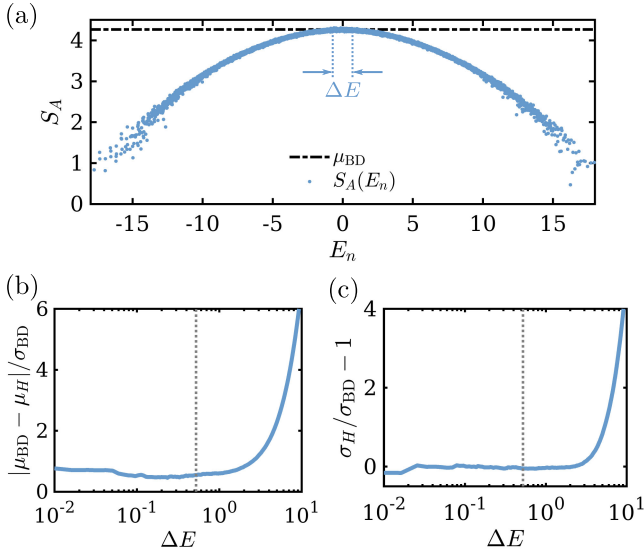
FIG. 9. (a) Eigenstate entanglement entropy of the MFIM for model parameters $g = 1.08$, $h = 0.3$, and $L = 14$. The parameter ΔE quantifies the energy window from which the variance of S_A is computed. (b) Mean and (c) standard deviation of the entanglement entropy distribution as a function of the energy window width ΔE. The ΔE corresponding to a window of 600 eigenstates used in the main text is shown with vertical dotted lines.

discussed in the main text are quite insensitive to the choice of energy window width.

In Fig. 9(a), we show the distribution of entanglement entropy computed for the MFIM with the MC parameters $g = 1.08$ and $h = 0.3$ for $L = 14$. We compute the mean and variance of the distribution of S_A computed for midspectrum eigenstates and using a variable window ΔE ranging from $\Delta E = 10^{-2}$ (approximately the typical eigenstate-to-eigenstate energy difference) to $\Delta E = 10$ (approximately half the bandwidth of the system). We find that the mean and variance of the distribution do not vary significantly if $\Delta E \lesssim 2$. In the main text, we employ a total of 600 eigenstates for $L = 14$ (see vertical dotted lines), which is a tiny fraction of the total number of states $2^{14} = 16384$. We repeat the same analysis for all system sizes to define the width of the windows used in the main text for all system sizes L.

APPENDIX C: FLUCTUATIONS OF EE AS A FUNCTION OF FRC GATE RANGE AND PERIOD

In Fig. 2 of the main text, we found deviations from RMT in the second moment of the EE distribution of eigenstates that persist with increasing L. These differences were attributed to locality, the only feature present in the FRC. We now generalize the FRC model discussed in Sec. III by relaxing the constraint of locality in order to observe the convergence to RMT. This observation will be achieved (a) by increasing the range of the local gates and (b) by increasing the number of periods of the FRC. As

such, the circuit structure will be labeled by two parameters: the range r and the period T, discussed in turn below.

We consider brickwork circuits with staggered layers of range-r unitary gates acting on a periodic one-dimensional spin-1/2 chain of length L. The range r is the number of contiguous qubits each individual gate acts on, so $U_{j,j+1,\ldots,j+(r-1)}$ acts on sites $(j, j+1, \ldots, j+r-1)$. Thus, $r = 2$ denotes nearest-neighbor gates while $r = 3$ is a three-site gate including both nearest and next-nearest neighbor interactions. The matrix $U_{j,j+1,\ldots,j+(r-1)}$ is a random $U(n)$ matrix, with $n = 2^r$.

The generalized circuit architecture has a periodic brickwork layout with variable period $T \in \mathbb{Z}$. The circuit implements discrete time evolution, and advancing by one unit of time comprises the application of a "layer" comprised of r staggered sublayers. Each sublayer is displaced by one lattice site with respect to the prior sublayer. For example, for the $r = 2$ considered in the main text, advancing by one unit of time entails applying one layer of even and odd gates:

$$U(t+1, t) = \underbrace{\prod_j U_{2j+1,2j+2}(t)}_{U_{\mathrm{odd}}(t) \equiv U_1(t)} \underbrace{\prod_i U_{2i,2i+1}(t)}_{U_{\mathrm{even}}(t) \equiv U_0(t)}. \quad \text{(C1)}$$

Likewise, $r = 3$ requires applying three staggered sublayers of gates starting from the $(0, 1, 2)$, $(1, 2, 3)$, and $(2, 3, 4)$ bonds, respectively:

$$U(t+1, t) = \underbrace{\prod_k U_{3k+2,3k+3,3k+4}(t)}_{U_2(t)} \underbrace{\prod_j U_{3j+1,3j+2,3j+3}(t)}_{U_1(t)}$$

$$\times \underbrace{\prod_i U_{3i,3i+1,3i+2}(t)}_{U_0(t)}. \quad \text{(C2)}$$

More generally, for range r gates,

$$U(t+1, t) = \prod_{\alpha=0}^{r-1} U_\alpha(t),$$

$$U_\alpha(t) = \prod_j U_{rj+\alpha,rj+\alpha+1,\ldots,rj+\alpha+r-1}. \quad \text{(C3)}$$

In cases where L is not divisible by r, we act with an identity matrix on the remaining sites. For a circuit with periodicity T, the gates in the first T layers are chosen independently, and layers repeat after T time steps: $U(t+T+1, t+T) = U(t+1, t)$. The generalized Floquet unitary is defined as the time-evolution operator for period T:

$$U_G(r, T) = \prod_{t=0}^{T-1} U(t+1, t), \quad \text{(C4)}$$
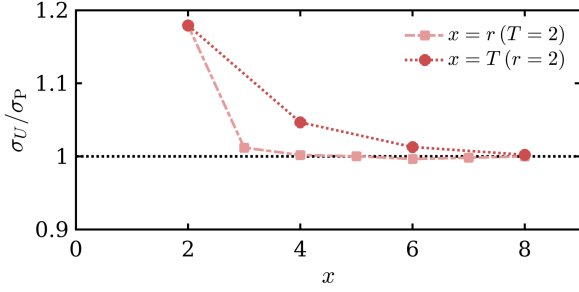
and $U(t = nT, 0) = U_G(r, T)^n$.

FIG. 10.   Convergence of the EE standard deviation of FRC eigenstates, σ_U, to the RMT prediction as a function of gate range r for fixed circuit depth T (squares), and as a function of circuit depth T for a fixed gate range (circles). Here, we use a system of $L = 16$ qubits.

FIG. 11.   Color maps of midspectrum entanglement entropy fluctuations normalized with σ_{BD}, computed for the MFIM with transverse field g and longitudinal field h, for $L = 14$. We note that the color map agrees qualitatively with the conclusions obtained form D_{KL} in Fig. 4(a) of the main text.

Figure 10 shows that the second moment of the EE distribution of eigenstates, σ_U, converges towards the RMT value σ_P both by increasing the period of the FRC (varying T while fixing $r = 2$) or by increasing the range of the gates (varying r while fixing $T = 2$). These results corroborate the expectation that reducing locality increases convergence to RMT. However, it is striking that just increasing the gate range from $r = 2$ to $r = 3$ is already enough to remove most of the observed difference in standard deviation, suggesting that other (more sensitive) metrics might be needed to probe deviations from RMT.

APPENDIX D: FLUCTUATIONS OF EE AS A FUNCTION OF HAMILTONIAN MODEL PARAMETERS

Since in most of the parameter space away from the MC point the main contribution to D_{KL} comes from the first moment, which refers to the choice of the BD distribution, we now also present an alternate but related diagnostic of chaos that is agnostic to the reference RMT distribution and only looks at the (normalized) fluctuations of EE: $\sigma_H/\sqrt{2^{-L}}$. This ratio is expected to be system-size independent and minimized for maximally chaotic systems while being exponentially increasing for L for near-integrable systems. In this way, maximally chaotic Hamiltonians can be identified by minimizing the value of σ_H, even if the correct reference distribution is unknown. In Fig. 11, we show the normalized standard deviation of the microcanonical fluctuations of EE of eigenstates as a function of (g, h). Similarly to Fig. 4(a) of the main text, which accounts for both moments of the EE distribution, we find that σ_H reaches a global minimum at the MC parameters and shows qualitatively similar behavior as D_{KL} away from the MC point. The color map appears more noisy than Fig. 4(a) because second moments have larger statistical fluctuations than first moments.
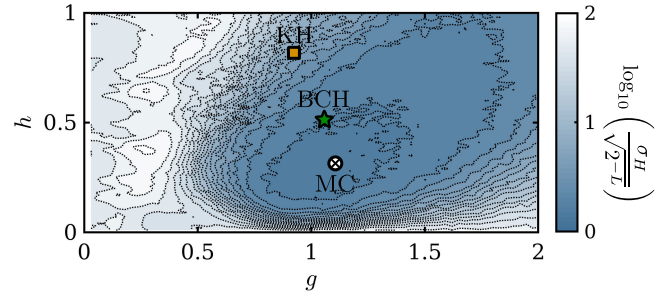
APPENDIX E: DISTRIBUTION OF EE FOR SOME STANDARD PARAMETER VALUES OF THE MFIM

The MFIM is a paradigmatic model of a strongly quantum chaotic system and has been routinely used in the study of quantum thermalization. In particular, there are several standard sets of model parameters that are believed to be strongly chaotic. In this appendix, we compare the distribution of entanglement entropy for the most chaotic point found in the main text and previously used parameters in the literature. Figure 12(a) shows histograms for the entanglement entropy of midspectrum eigenstates for (i) the MC parameters of Fig. 4, $(g, h) = (1.08, 0.30)$ (blue bars), (ii) the BCH model [48] (green bars), $(g, h) = (1.05, -0.5)$, and (iii) the Kim-Huse model, $(g, h) = ((\sqrt{5}+5)/8, (\sqrt{5}+1)/4) \approx (0.9045, 0.8090)$ [49] (red bars). We find that the BCH parameters agree reasonably well with the BD distribution, whereas the KH parameter strongly deviates by more than 2 standard deviations.

A more refined look into the distribution of entanglement entropy normalized with the BD distribution is shown in Figs. 12(b) and 12(c). We observe that, within the scale of σ_{BD}, eigenstates in the BCH model agree well with RMT behavior: The means of the EE distributions differ by $\Delta\mu \sim \sigma_{BD}$. In contrast, for the KH parameters, we observe large deviations between the EE distribution of eigenstates and random states: In this case, the means differ by $\Delta\mu \sim 5\sigma_{BD}$, and the standard deviation is around 5 times larger.

APPENDIX F: QUANTIFYING QUANTUM CHAOS THROUGH THE SECOND RENYI ENTROPY

In the main text, we used the von Neumann entanglement entropy S_A of quantum state ensembles (eigenstates and constrained RMT ensembles) to quantify quantum
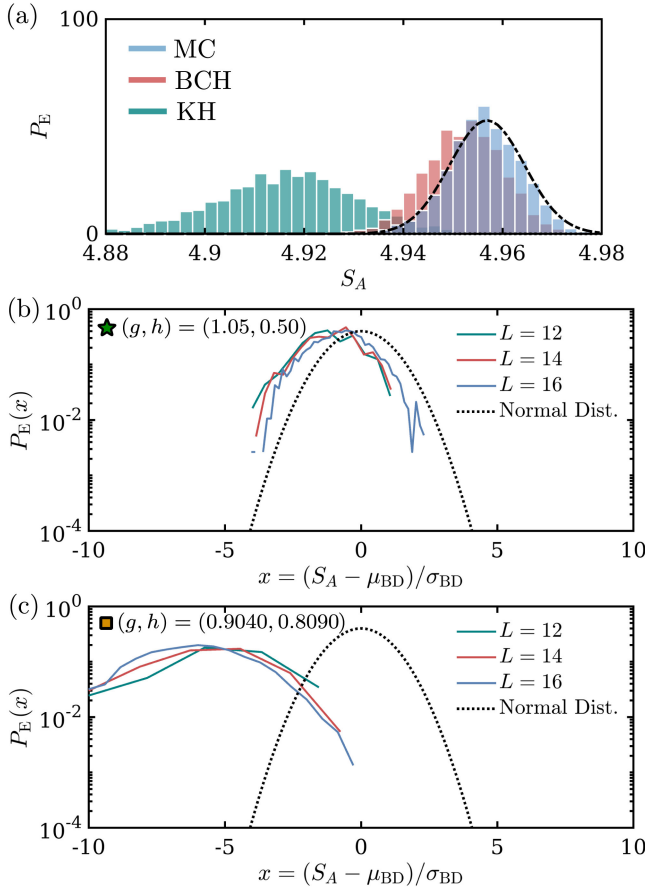
FIG. 12. (a) Distribution of entanglement for typically used values of the MFIM: MC parameters in the present work (blue), the Banuls-Cirac-Hastings model (red), and Kim-Huse (green). The BD distribution is shown with a dotted-dashed line. Histogram of midspectrum EE obtained for the (b) BCH and (c) KH parameters as a function of system size, showing deviations from RMT behavior that persist in the thermodynamic limit. The reference standard normal distribution is shown with dotted lines.
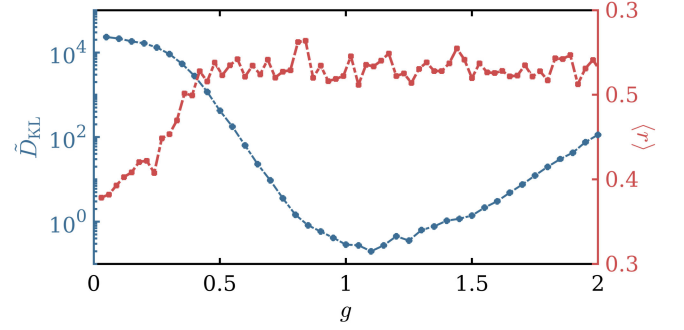

FIG. 13. Modified KL divergence $\tilde{D}_{KL}$ obtained from the distributions of the second Renyi entropy, $S_2 = -\log(\mathrm{Tr}[\rho_A^2])$, of eigenstates and constrained RMT ensembles [cf. Fig. 4(c) of the main text, which was obtained using the von Neumann EE]. Data are shown for the MFIM along the MC linecut ($h = 0.3$) and as a function of transverse field g, for $L = 14$. Also shown is the ratio factor $\langle r \rangle$ for the same model parameters.

Figure 13 shows the value of $\tilde{D}_{KL}$ as a function of transverse field at the MC linecut ($h = 0.3$) and for $L = 14$. We find that the behavior of $\tilde{D}_{KL}$ agrees remarkably well with that obtained using the von Neumann EE that was discussed in the main text; see Fig. 4(c). In particular, the entanglement behavior (as measured through S_2) of the microcanonical ensemble of eigenstates agrees with the constrained RMT ensemble in fine-tuned regions of parameter space around $g = 1.05$ and $h = 0.3$. This finding shows that our conclusions are insensitive to the entanglement observable of choice.

chaos. We also argued that the choice of entanglement observable is not particularly important for the purposes of our work. To show that this is the case, we compute D_{KL} using the second Renyi entropy, $S_2 = -\log(\mathrm{Tr}[\rho_A^2])$ of the quantum state ensembles, rather than S_A.

To generate the reference distribution of constrained random states, we first sample over $N = 10^4$ pure random states constrained to the largest (midspectrum) symmetry sector of the $U(1)$ charge and then use these samples to compute the moments of the second Renyi entropy. In the case of the microcanonical eigenstate ensemble, the moments of S_2 are computed using eigenstates of the MFIM. We use the same number of eigenstates that was used in the main text. We then define the modified metric of distance between ensembles using

$$\tilde{D}_{KL}(P_E, P_R) = \int dS_2 P_E(S_2) \log \frac{P_E(S_2)}{P_R(S_2)}. \quad (F1)$$

[1] J. M. Deutsch, *Quantum statistical mechanics in a closed system*, Phys. Rev. A **43**, 2046 (1991).

[2] Mark Srednicki, *Chaos and quantum thermalization*, Phys. Rev. E **50**, 888 (1994).

[3] Marcos Rigol, Vanja Dunjko, and Maxim Olshanii, *Thermalization and its mechanism for generic isolated quantum systems*, Nature (London) **452**, 854 (2008).

[4] Rahul Nandkishore and David A Huse, *Many-body localization and thermalization in quantum statistical mechanics*, Annu. Rev. Condens. Matter Phys. **6**, 15 (2015).

[5] S. Trotzky, Y.-A. Chen, A. Flesch, I. P. McCulloch, U. Schollwöck, J. Eisert, and I. Bloch, *Probing the relaxation towards equilibrium in an isolated strongly correlated one-dimensional Bose gas*, Nat. Phys. **8**, 325 (2012).

[6] Adam M. Kaufman, M. Eric Tai, Alexander Lukin, Matthew Rispoli, Robert Schittko, Philipp M. Preiss, and Markus Greiner, *Quantum thermalization through entanglement in an isolated many-body system*, Science **353**, 794 (2016).

[7] Yijun Tang, Wil Kao, Kuan-Yu Li, Sangwon Seo, Krishnanand Mallayya, Marcos Rigol, Sarang Gopalakrishnan, and Benjamin L. Lev, *Thermalization near integrability in a dipolar quantum Newton's cradle*, Phys. Rev. X **8**, 021030 (2018).

[8] Govinda Clos, Diego Porras, Ulrich Warring, and Tobias Schaetz, *Time-resolved observation of thermalization in an isolated quantum system*, Phys. Rev. Lett. **117,** 170401 (2016).

[9] Hyosub Kim, YeJe Park, Kyungtae Kim, H.-S. Sim, and Jaewook Ahn, *Detailed balance of thermalization dynamics in Rydberg-atom quantum simulators*, Phys. Rev. Lett. **120,** 180502 (2018).

[10] Y. Y. Atas, E. Bogomolny, O. Giraud, and G. Roux, *The distribution of the ratio of consecutive level spacings in random matrix ensembles*, Phys. Rev. Lett. **110,** 084101 (2013).

[11] Y. Y. Atas, E. Bogomolny, O. Giraud, P. Vivo, and E. Vivo, *Joint probability densities of level spacing ratios in random matrices*, J. Phys. A **46,** 355204 (2013).

[12] Vadim Oganesyan and David A. Huse, *Localization of interacting fermions at high temperature*, Phys. Rev. B **75,** 155111 (2007).

[13] Bruno Bertini, Pavel Kos, and Tomaž Prosen, *Exact spectral form factor in a minimal model of many-body quantum chaos*, Phys. Rev. Lett. **121,** 264101 (2018).

[14] Hrant Gharibyan, Masanori Hanada, Stephen H. Shenker, and Masaki Tezuka, *Onset of random matrix behavior in scrambling systems*, J. High Energy Phys. 7 (2018) 124.

[15] Amos Chan, Andrea De Luca, and John T. Chalker, *Solution of a minimal model for many-body quantum chaos*, Phys. Rev. X **8,** 041019 (2018).

[16] Amos Chan, Andrea De Luca, and J. T. Chalker, *Spectral statistics in spatially extended chaotic quantum many-body systems*, Phys. Rev. Lett. **121,** 060601 (2018).

[17] Aaron J. Friedman, Amos Chan, Andrea De Luca, and J. T. Chalker, *Spectral statistics and many-body quantum chaos with conserved charge*, Phys. Rev. Lett. **123,** 210603 (2019).

[18] S. J. Garratt and J. T. Chalker, *Local pairing of Feynman histories in many-body Floquet models*, Phys. Rev. X **11,** 021051 (2021).

[19] James R. Garrison and Tarun Grover, *Does a single eigenstate encode the full Hamiltonian?*, Phys. Rev. X **8,** 021026 (2018).

[20] Tsung-Cheng Lu and Tarun Grover, *Renyi entropy of chaotic eigenstates*, Phys. Rev. E **99,** 032111 (2019).

[21] Luca D'Alessio, Yariv Kafri, Anatoli Polkovnikov, and Marcos Rigol, *From quantum chaos and eigenstate thermalization to statistical mechanics and thermodynamics*, Adv. Phys. **65,** 239 (2016).

[22] Joshua M. Deutsch, *Eigenstate thermalization hypothesis*, Rep. Prog. Phys. **81,** 082001 (2018).

[23] Anatoly Dymarsky, Nima Lashkari, and Hong Liu, *Subsystem ETH*, Phys. Rev. E **97,** 012140 (2018).

[24] Mark Srednicki, *The approach to thermal equilibrium in quantized chaotic systems*, J. Phys. A **32,** 1163 (1999).

[25] Luca D'Alessio, Yariv Kafri, Anatoli Polkovnikov, and Marcos Rigol, *From quantum chaos and eigenstate thermalization to statistical mechanics and thermodynamics*, Adv. Phys. **65,** 239 (2016).

[26] Lev Vidmar and Marcos Rigol, *Entanglement entropy of eigenstates of quantum chaotic Hamiltonians*, Phys. Rev. Lett. **119,** 220603 (2017).

[27] Chaitanya Murthy and Mark Srednicki, *Structure of chaotic eigenstates and their entanglement entropy*, Phys. Rev. E **100,** 022131 (2019).

[28] Eugenio Bianchi, Lucas Hackl, Mario Kieburg, Marcos Rigol, and Lev Vidmar, *Volume-law entanglement entropy of typical pure quantum states*, PRX Quantum **3,** 030201 (2022).

[29] We may henceforth drop these qualifiers (local, physical), but, throughout this work, we will only consider Hamiltonians with short-range, few-body interactions represented by sparse matrices. For Floquet systems, the interactions are time dependent but still instantaneously local.

[30] Don N. Page, *Average entropy of a subsystem*, Phys. Rev. Lett. **71,** 1291 (1993).

[31] Eugenio Bianchi and Pietro Donà, *Typical entanglement entropy in the presence of a center: Page curve and its variance*, Phys. Rev. D **100,** 105010 (2019).

[32] Lev Vidmar, Lucas Hackl, Eugenio Bianchi, and Marcos Rigol, *Entanglement entropy of eigenstates of quadratic fermionic Hamiltonians*, Phys. Rev. Lett. **119,** 020601 (2017).

[33] Siddhardh C. Morampudi, Anushya Chandran, and Chris R. Laumann, *Universal entanglement of typical states in constrained systems*, Phys. Rev. Lett. **124,** 050602 (2020).

[34] Masudul Haque, Paul A. McClarty, and Ivan M. Khaymovich, *Entanglement of midspectrum eigenstates of chaotic many-body systems: Reasons for deviation from random ensembles*, Phys. Rev. E **105,** 014109 (2022).

[35] Yichen Huang, *Universal eigenstate entanglement of chaotic local Hamiltonians*, Nucl. Phys. **B938,** 594 (2019).

[36] Yichen Huang, *Universal entanglement of mid-spectrum eigenstates of chaotic local Hamiltonians*, Nucl. Phys. **B966,** 115373 (2021).

[37] Yichen Huang, *Deviation from maximal entanglement for mid-spectrum eigenstates of local Hamiltonians*, arXiv:2202.01173.

[38] M. Kliczkowski, R. Świętek, L. Vidmar, and M. Rigol, *Average entanglement entropy of midspectrum eigenstates of quantum-chaotic interacting Hamiltonians*, Phys. Rev. E **107,** 064119 (2023).

[39] Anatoly Dymarsky, *Bound on eigenstate thermalization from transport*, Phys. Rev. Lett. **128,** 190601 (2022).

[40] Jiaozi Wang, Mats H. Lamann, Jonas Richter, Robin Steinigeweg, Anatoly Dymarsky, and Jochen Gemmer, *Eigenstate thermalization hypothesis and its deviations from random-matrix theory beyond the thermalization time*, Phys. Rev. Lett. **128,** 180601 (2022).

[41] Jonas Richter, Anatoly Dymarsky, Robin Steinigeweg, and Jochen Gemmer, *Eigenstate thermalization hypothesis beyond standard indicators: Emergence of random-matrix behavior at small frequencies*, Phys. Rev. E **102,** 042127 (2020).

[42] Marlon Brenes, Silvia Pappalardi, Mark T. Mitchison, John Goold, and Alessandro Silva, *Out-of-time-order correlations and the fine structure of eigenstate thermalization*, Phys. Rev. E **104,** 034120 (2021).

[43] Laura Foini and Jorge Kurchan, *Eigenstate thermalization hypothesis and out of time order correlators*, Phys. Rev. E **99,** 042139 (2019).

[44] Amos Chan, Andrea De Luca, and J. T. Chalker, *Eigenstate correlations, thermalization, and the butterfly effect*, Phys. Rev. Lett. **122,** 220601 (2019).

[45] Xiao-Liang Qi and Daniel Ranard, *Determining a local Hamiltonian from a single eigenstate*, Quantum **3,** 159 (2019).

[46] Bruno Bertini, Pavel Kos, and Tomaz Prosen, *Entanglement spreading in a minimal model of maximal many-body quantum chaos*, Phys. Rev. X **9,** 021033 (2019).

[47] Sarang Gopalakrishnan and Austen Lamacraft, *Unitary circuits of finite depth and infinite width from quantum channels*, Phys. Rev. B **100,** 064309 (2019).

[48] M. C. Bañuls, J. I. Cirac, and M. B. Hastings, *Strong and weak thermalization of infinite nonintegrable quantum systems*, Phys. Rev. Lett. **106,** 050405 (2011).

[49] Hyungwon Kim and David A. Huse, *Ballistic spreading of entanglement in a diffusive nonintegrable system*, Phys. Rev. Lett. **111,** 127205 (2013).

[50] The notion of "degree of chaos" that we introduce is similar to that used in other contexts, for instance, in quantum circuits. In this case, it is known that Clifford gates and Haar gates generate quantum state distributions that agree at the level of first and second moments, but Haar random gates are closer to RMT behavior at the level of higher moments. In this sense, Clifford gates are considered to be "less chaotic" than Haar gates, even if they produce the same first two moments.

[51] Nicholas Hunter-Jones, *Unitary designs from statistical mechanics in random quantum circuits*, arXiv:1905.12053.

[52] Fernando G. S. L. Brandão, Wissam Chemissany, Nicholas Hunter-Jones, Richard Kueng, and John Preskill, *Models of quantum complexity growth*, PRX Quantum **2,** 030316 (2021).

[53] Jordan S. Cotler, Daniel K. Mark, Hsin-Yuan Huang, Felipe Hernandez, Joonhee Choi, Adam L. Shaw, Manuel Endres, and Soonwon Choi, *Emergent quantum state designs from individual many-body wavefunctions*, PRX Quantum **4,** 010311 (2023).

[54] Joonhee Choi, Adam L. Shaw, Ivaylo S. Madjarov, Xin Xie, Ran Finkelstein, Jacob P. Covey, Jordan S. Cotler, Daniel K. Mark, Hsin-Yuan Huang, Anant Kale, Hannes Pichler, Fernando G. S. L. Brandão, Soonwon Choi, and Manuel Endres, *Emergent quantum randomness and benchmarking from Hamiltonian many-body dynamics*, Nature (London) **613,** 468 (2023).

[55] Wen Wei Ho and Soonwon Choi, *Exact emergent quantum state designs from quantum chaotic dynamics*, Phys. Rev. Lett. **128,** 060601 (2022).

[56] Matteo Ippoliti and Wen Wei Ho, *Solvable model of deep thermalization with distinct design times*, Quantum **6,** 886 (2022).

[57] RE Prange, *The spectral form factor is not self-averaging*, Phys. Rev. Lett. **78,** 2280 (1997).

[58] Francesca Pietracaprina, Nicolas Macé, David J. Luitz, and Fabien Alet, *Shift-invert diagonalization of large many-body localizing spin chains*, SciPost Phys. **5,** 045 (2018).

[59] David J. Luitz, *Polynomial filter diagonalization of large Floquet unitary operators*, SciPost Phys. **11,** 021 (2021).

[60] Mohit Pandey, Pieter W. Claeys, David K. Campbell, Anatoli Polkovnikov, and Dries Sels, *Adiabatic eigenstate deformations as a sensitive probe for quantum chaos*, Phys. Rev. X **10,** 041017 (2020).

[61] Pierpaolo Vivo, Mauricio P. Pato, and Gleb Oshanin, *Random pure states: Quantifying bipartite entanglement beyond the linear statistics*, Phys. Rev. E **93,** 052106 (2016).

[62] Lu Wei, *Proof of Vivo-Pato-Oshanin's conjecture on the fluctuation of von Neumann entropy*, Phys. Rev. E **96,** 022106 (2017).

[63] As a side remark, we note that the orthogonality of eigenstates is not responsible for the deviation from RMT, as discussed in Ref. [34]. Indeed, we checked that the distribution of entanglement entropy produced by a global $U(N)$ random unitary (i.e., in the absence of locality) does not exhibit deviations from the Page distribution for the first two moments.

[64] Alexander Lukin, Matthew Rispoli, Robert Schittko, M. Eric Tai, Adam M. Kaufman, Soonwon Choi, Vedika Khemani, Julian Léonard, and Markus Greiner, *Probing entanglement in a many-body localized system*, Science **364,** 256 (2019).

[65] Pierpaolo Vivo, *Entangled random pure states with orthogonal symmetry: Exact results*, J. Phys. A **43,** 405206 (2010).

[66] Santosh Kumar and Akhilesh Pandey, *Entanglement in random pure states: Spectral density and average von Neumann entropy*, J. Phys. A **44,** 445301 (2011).

[67] We have checked that our results are not qualitatively changed on using these analytic reference values, as compared to using numerically determined moments for real random constrained states.

[68] Itai Arad, Tomotaka Kuwahara, and Zeph Landau, *Connecting global and local energy distributions in quantum spin models on a lattice*, J. Stat. Mech. (2016) 033301.

[69] The results are not sensitive to the value of the symmetry-breaking field.

[70] T. D. Schultz, D. C. Mattis, and E. H. Lieb, *Two-dimensional Ising model as a soluble problem of many fermions*, Rev. Mod. Phys. **36,** 856 (1964).

[71] Liangsheng Zhang, Hyungwon Kim, and David A. Huse, *Thermalization of entanglement*, Phys. Rev. E **91,** 062128 (2015).

[72] Daniel A. Roberts, Douglas Stanford, and Leonard Susskind, *Localized shocks*, J. High Energy Phys. 03 (2015) 051.

[73] Vedika Khemani, Ashvin Vishwanath, and David A. Huse, *Operator spreading and the emergence of dissipative hydrodynamics under unitary evolution with conservation laws*, Phys. Rev. X **8,** 031057 (2018).

[74] Andreas Elben, Steven T. Flammia, Hsin-Yuan Huang, Richard Kueng, John Preskill, Benoît Vermersch, and Peter Zoller, *The randomized measurement toolbox*, Nat. Rev. Phys. **5,** 9 (2023).

[75] A. Elben, B. Vermersch, M. Dalmonte, J. I. Cirac, and P. Zoller, *Rényi entropies from random quenches in atomic Hubbard and spin models*, Phys. Rev. Lett. **120,** 050406 (2018).

[76] Tiff Brydges, Andreas Elben, Petar Jurcevic, Benoît Vermersch, Christine Maier, Ben P. Lanyon, Peter Zoller, Rainer Blatt, and Christian F. Roos, *Probing Renyi*

entanglement entropy via randomized measurements, Science **364**, 260 (2019).

[77] Andreas Elben, Richard Kueng, Hsin-Yuan (Robert) Huang, Rick van Bijnen, Christian Kokail, Marcello Dalmonte, Pasquale Calabrese, Barbara Kraus, John Preskill, Peter Zoller, and Benoît Vermersch, *Mixed-state entanglement from local randomized measurements*, Phys. Rev. Lett. **125**, 200501 (2020).

[78] Aniket Rath, Cyril Branciard, Anna Minguzzi, and Benoît Vermersch, *Quantum fisher information from randomized measurements*, Phys. Rev. Lett. **127**, 260501 (2021).

[79] Steven T. Flammia and Yi-Kai Liu, *Direct fidelity estimation from few Pauli measurements*, Phys. Rev. Lett. **106**, 230501 (2011).

[80] Lata Kh Joshi, Andreas Elben, Amit Vikram, Benoît Vermersch, Victor Galitski, and Peter Zoller, *Probing many-body quantum chaos with quantum simulators*, Phys. Rev. X **12**, 011018 (2022).

[81] Hsin-Yuan Huang, Yu Tong, Di Fang, and Yuan Su, *Learning many-body Hamiltonians with Heisenberg-limited scaling*, Phys. Rev. Lett. **130**, 200403 (2023).

[82] Kshiti Sneh Rai, J. Ignacio Cirac, and Álvaro M. Alhambra, *Matrix product state approximations to quantum states of low energy variance*, arXiv:2307.05200.

[83] Klée Pollock, Peter P. Orth, and Thomas Iadecola, *Variational microcanonical estimator*, Phys. Rev. Res. **5**, 033224 (2023).

[84] Madan Lal Mehta, *Random Matrices*, 3rd ed. (Elsevier Inc., San Diego, CA, 2004).